

Primary Neuronal Degeneration in the Guinea Pig
Effects on Spontaneous Rate-Type

by

Adam C. Furman

B.S.E Bioengineering
The University of Pennsylvania, 2003

ARCHIVED

SUBMITTED TO
THE HARVARD-MIT DIVISION OF HEALTH SCIENCES AND TECHNOLOGY IN
PARTIAL FULFILLMENT OF THE REQUIREMENTS FOR THE DEGREE OF

DOCTOR OF PHILOSOPHY IN
HEALTH SCIENCES AND TECHNOLOGY
AT THE
MASSACHUSETTS INSTITUTE OF TECHNOLOGY

FEBRUARY 2013

© 2013 Adam Furman. All rights reserved.

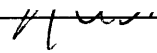
The author hereby grants to MIT permission to reproduce
and to distribute publicly paper and electronic
copies of this thesis document in whole or in part
in any medium now known or hereafter created.

Signature of Author:



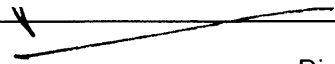
Harvard-MIT Division of Health Sciences and Technology
October 3, 2012

Certified by:



M. Charles Liberman, Ph.D.
Harold Schuknecht Professor of Otolaryngology, Harvard Medical School
Director of the Eaton-Peabody Laboratory, Mass. Eye & Ear Infirmary
Thesis Supervisor

Accepted by:



Arup Chakraborty, Ph.D.
Director, Institute for Medical Engineering and Sciences
Robert T. Haslam Professor of Chemical Engineering, Chemistry and Biological Engineering
Massachusetts Institute of Technology

Primary Neuronal Degeneration in the Guinea Pig:
Effects on Spontaneous Rate-Type

Adam C. Furman

Submitted to the Harvard-MIT Division of Health Sciences and Technology
on October 3, 2012 in partial fulfillment of the
Requirements of the Degree of Doctor of Philosophy in
Health Sciences and Technology
Thesis Supervisor: M. Charles Liberman, Ph.D.

Acoustic overexposure can cause death of cochlear nerve fibers, even if elevations in cochlear sensitivity are reversible and even if there is no hair cell loss. We hypothesized that this primary neural degeneration does not raise cochlear thresholds because it is selective for cochlear neurons with high thresholds and low spontaneous rates (SRs). We tested this hypothesis by recording from single cochlear neurons in guinea pigs and evaluating neuronal degeneration via confocal microscopy 14 days after exposure to noise (4-8kHz, 106dB SPL, 2 hrs).

Suprathreshold amplitudes of otoacoustic emissions recovered post-exposure, suggesting complete hair cell recovery; suprathreshold amplitudes of the auditory brainstem response remained attenuated for high-frequency stimuli, consistent with primary neural degeneration in the basal half of the cochlea. Single-fiber recordings from exposed animals showed that all sound-evoked response properties, including threshold, sharpness of tuning, maximum discharge rate, dynamic range, response adaptation, and recovery from forward masking, were indistinguishable from responses recorded from unexposed controls. The only physiological abnormalities were revealed in the population statistics: in high-frequency regions where low-SR (<20sp/sec) fibers are 47% of the control ear, that number was reduced to 29% in the exposed ear.

Cochlear afferent synapses were counted after immunostaining for juxtaposed pre-synaptic ribbons and post-synaptic glutamate receptor patches in the inner hair cell area. The observed 20% synapse loss throughout the basal half of the cochlea was consistent with the physiological data. Analysis of synaptic morphology suggested remaining pre-synaptic ribbons were hypertrophied and membrane localization of post-synaptic glutamate receptors was reduced. The significance of the ribbon hypertrophy is unclear, but reduced receptor expression may represent receptor internalization, suggested as a mechanism to minimize the glutamate excitotoxicity that underlies this noise-induced degeneration.

In the normal ear, fibers with high thresholds and low SRs are relatively insensitive to masking, thus are important for hearing in a noisy environment. We speculate that over a lifetime of repeated moderate noise exposure, the typical human ear may selectively lose these low-SR fibers and that this selective neuropathy may be an important contributor to the well-known problems with hearing-in-noise in the aging ear.

Table of Contents

Figure Reference.....	6
1 Acronyms Used	7
2 Introduction and Background	7
2.1 Hearing and Hearing Damage	7
2.2 A Novel Sound-Exposure Paradigm.....	9
2.3 Single Fiber Recordings and Spontaneous Rate Classifications.....	11
2.4 Synaptic Ribbons and Spontaneous Rate	13
2.5 Forward Masking	13
3 Specific Aims and Rationale	15
4 Methods	17
4.1 Animals and Groups.....	17
4.2 Noise Exposure	17
4.3 ABR and DPOAE Measures	17
4.4 Anesthesia and Surgical Preparation	18
4.5 CAP Thresholds and Forward Masking Functions.....	19
4.6 Recording of Single Fibers.....	20
4.7 Histological Analysis	21
4.7.1 Tissue Fixation.....	21
4.7.2 Microdissection and Immunological Staining.....	21
4.7.3 Microscopy and Image Analysis	22
5 Results	24
5.1 Noise Exposure and Cochlear Function	24
5.1.1 ABR and DPOAE Recovery	24
5.1.2 ABR Wave-1 Phenotype	27
5.2 Single Fiber Responses	27
5.2.1 Tuning Curves and Spontaneous Rate.....	27
5.2.2 Thresholds at CF	28
5.2.3 Spontaneous Rate Distributions	30
5.2.4 Other Response Properties	33
5.3 Forward Masking	37
5.3.1 Forward Masking at the Single Fiber Level.....	37
5.3.2 Forward Masking in the CAP.....	40
5.3.3 Low- and High-SR Contributions to the CAP.....	42
5.4 Histology of Ribbon Loss.....	43
5.4.1 Confocal Imaging.....	43
5.4.2 Spatial Distribution of Ribbons.....	47
5.4.3 Synaptic Ribbons and Post-Synaptic Markers	52
6 Discussion	55
6.1 Preservation of Threshold	55

6.2	ABR wave-1 Amplitude and Loss of Synapses.....	55
6.3	Low-SR Losses	57
6.4	Glutamate Excitotoxicity.....	58
6.5	Forward Masking	59
6.6	A Disrupted Synapse – Comparisons between Physiology and Morphology.....	60
7	Conclusions and Summary	61
8	Acknowledgements	61
9	List of References.....	63

Figure Reference

Figure 1 The afferent innervation of the inner hair cell.....	9
Figure 2 Threshold shift and recovery following 2-hr exposure to 106 dB noise.....	10
Figure 3 Slow degeneration of spiral ganglion cells after reversible noise-induced threshold shift.....	11
Figure 4 Spontaneous rate and threshold at the CF in single AN fibers	13
Figure 5 DPOAE thresholds and suprathreshold amplitudes recover after exposure to the 106 dB noise band	25
Figure 6 ABR thresholds recover at high frequencies after exposure, but wave-1 amplitudes do not.....	26
Figure 7 AN Tuning curves appear unchanged post exposure.....	28
Figure 8 Thresholds at CF vs CF for control and exposed ears	29
Figure 9 Mean CAP thresholds are normal post-exposure	30
Figure 10 Spontaneous rate distributions suggest a selective loss of low-SR fibers in the basal half of the cochlea.....	32
Figure 11 The relation between threshold and SR is maintained in exposed ears	33
Figure 12 Tuning and dynamic range of AN fibers remain unchanged in the exposed ears.....	35
Figure 13 Basic properties of the PSTHs in response to CF tone bursts remain unchanged in the exposed ears.....	36
Figure 14 Forward masking analysis in single AN Fibers	38
Figure 15 Forward masking recovery time is unchanged in exposed ears.....	39
Figure 16 CAP Forward Masking Analysis	41
Figure 17 CAP Forward Masking functions are unchanged in the exposed ears.....	42
Figure 18 Modeling the Low- and High-SR contributions to CAP forward masking functions.....	43
Figure 19 Confocal analysis of noise-induced synaptic degeneration.	45
Figure 20 Synaptic ribbon counts are reduced in noise-damaged cochlear regions.....	47
Figure 21 Illustration of the spatial transformations applied to assess the spatial organization of synaptic puncta on the pillar vs. modiolar sides of the IHC.	48
Figure 22 Ribbon volume is increased, and the normal modiolar-pillar gradient is disrupted, in noise-damaged cochlear regions.	50
Figure 23 The volume of glutamate receptor patches is reduced throughout much of the noise-exposed cochlea.	51
Figure 24 Analysis of the pairing of pre-synaptic ribbons with post-synaptic receptors	53
Figure 25 The frequency of orphan ribbons or glutamate receptors was increased in the noise-damaged cochlear regions.....	54

1 Acronyms Used

ABR – Auditory Brainstem Responses

AN – Auditory Nerve

CAP – Compound Action Potential

CF – Characteristic Frequency

DPOAE – Distortion Product Otoacoustic Emissions

EM – Electron Microscopy

IHC – Inner Hair Cell

PSTH – Post Stimulus Time Histogram

SR – Spontaneous Rate

2 Introduction and Background

2.1 Hearing and Hearing Damage

The mammalian auditory system is complex and finely tuned, encoding sound waves in the air into neural activity in the fibers of the auditory nerve (AN). Environmental sound is captured by the external ear and funneled through the tympanic membrane and middle ear, vibrating the stapes and creating a traveling wave inside the cochlea. Passive mechanical filtering and active amplification separate incoming sound into its frequency components, activating different portions of the cochlea tuned to different frequencies (Geisler, 1998). Along the entire length of the cochlea are sensory cells, the inner hair cells (IHCs, Figure 1A), that detect vibration within the cochlea with stereocilia bundles at their apical surface. Deflection of these stereocilia depolarizes the IHCs, triggering the release neurotransmitter into the synaptic cleft, putatively glutamate. This neurotransmitter release is mediated by synaptic ribbons, which are presynaptic specializations necessary for the coordinated release of glutamate-filled vesicles (Liberman, 1980; Khimich et al., 2005) (see Figure 1B). The release of neurotransmitter leads to the generation of action potentials in an AN fiber. The response of AN fibers ascends through several nuclei of the brainstem, midbrain and cortex, to eventually elicit an auditory percept (Geisler, 1998). However, not all AN fibers are the same; one way they can be classified is by their spontaneous rate (SR) of firing. Fibers with a low-SR predominately innervate the modiolar side of the IHC and have high thresholds in response to sound. High-SR fibers innervate the pillar side of the IHC and have the lowest thresholds (Liberman, 1980).

The auditory transduction pathway relies on the proper functioning of its intermediary steps. This pathway can be disrupted in a variety of ways, from normal use and aging, from viral and bacterial infections, and from exposure to ototoxic drugs. Exposure to loud noise can easily damage the auditory system, and early noise exposure may exacerbate age related hearing loss (Gates et al., 2000). Unfortunately, humans are normally exposed to a wide range of potentially damaging sounds every day, both at work at throughout daily life. Subway systems have intense squealing from wheels and brakes. Road construction uses jack hammers that are painfully loud even for people just walking past. Many neglect to wear hearing protection while using common tools around the house such as lawn mowers, leaf blowers, and power tools that can produce significant sound pressure levels. OSHA has set standards for exposure limits in the workplace, based upon permanent loss of auditory thresholds, but for years, exposures that only temporarily affected hearing threshold were considered to cause no permanent damage to the inner ear (OSHA, 2012).

Exposure to sufficiently intense sound causes substantial, non-reversible damage to the inner ear at the cellular level. Stereocilia and their tip links can be broken; hair cells and their supporting cells can degenerate (Robertson, 1982; Liberman and Dodds, 1984; Husbands et al., 1999). Depending on the severity of the exposure, damage can leave parts of the cochlea intact or cause temporary changes that recover with time. Moderate intensity sound exposures that are not severe enough to destroy hair cells cause swelling of synaptic terminals and subsequent retraction of dendritic endings within minutes after exposure (Pujol and Puel, 1999). Electron microscopy showed that this swelling disappeared within 1 – 2 days post-exposure, as the threshold was recovering, leading some authors to suggest that the dendritic damage was reversible and that hair cells were re-innervated by regenerating neurons within a few days following exposure (Puel et al., 1998; Pujol and Puel, 1999). However, neurons were never counted in these early studies on guinea pigs, and the inference that neurons had regenerated was based only on the observations that cochlear thresholds had returned to normal and terminal swelling had disappeared.

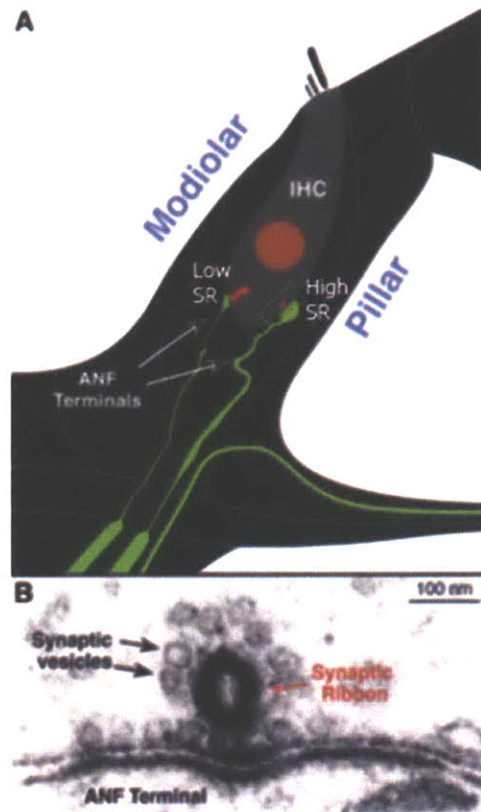


Figure 1 The afferent innervation of the inner hair cell.

(A) Schematic of afferent innervation to the inner hair cell (IHC). Synaptic ribbons (red) mediate the release of glutamate into the synapse. Low-Spontaneous Rate (SR) fibers innervate the modiolar side of the IHC, and high-SR fibers innervate the pillar side of the IHC. (B) An electron micrograph of the boxed synaptic region in (A). A synaptic ribbon is positioned near the pre-synaptic membrane. Tethered to it is a readily releasable pool of synaptic vesicles. Adapted with permission from (Liberian, 1980).

2.2 A Novel Sound-Exposure Paradigm

Recent studies in mouse have shown that a sound exposure that causes only a temporary threshold shift can lead to permanent neural degeneration (Kujawa and Liberman, 2009). In this study, the noise exposure was titrated such that the sound pressure level was high enough to produce a large temporary thresholds shift (i.e. 40-50 dB as measured 24 hrs post exposure) but low enough that the threshold shift was fully reversible within 1-2 weeks. Synaptic loss was quantified by counting synaptic ribbons and/or by counting spiral ganglion cells, the cell bodies of the AN. Since almost every AN synapse has precisely one pre-synaptic ribbon (Liberian, 1980), one can quantify synaptic degeneration by counting pre-synaptic ribbons in immunostained whole mounts of the cochlear sensory epithelium. Using this approach Kujawa and Liberman (2009) showed that these severe but reversible threshold shifts led to an immediate (within 1 day) loss of up to 50% of the AN synapses, followed over the course of

several months to a year by a commensurate loss of spiral ganglion cells. No loss of either inner or outer hair cells was ever seen in these ears. This light microscopic study in mouse suggested that the dendritic retraction observed in the EM studies of guinea pig was never reversed, and eventually led to the death of those neurons. Physiologically, the neural loss in mouse was correlated with a reduced suprathreshold amplitude of wave-1 of the auditory brainstem response (ABR), the summed responses of the AN fibers to a short tone pip. As further demonstration that the outer hair cells were intact and fully functional, it was shown that both the thresholds and the suprathreshold amplitudes of the distortion product otoacoustic emissions (DPOAEs) returned to pre-exposure values.

To demonstrate that the differences between the early EM studies (in guinea pig) and later confocal analysis (in mouse) were not due to species differences, this exposure “phenotype,” specifically the lack of threshold shift with a reduced suprathreshold amplitude of ABR wave-1 responses, was recreated in the guinea pig (Lin et al., 2011). These guinea pigs had large ABR and DPOAE threshold shifts 1-day post exposure (Figure 2), which fully recovered by 10 days post-exposure. These guinea pigs also had reduced numbers of synaptic ribbons 10 days post exposure. A micrograph of the spiral ganglion in these guinea pigs is shown in Figure 3. While the ganglion cells look normal shortly after exposure, months later there is substantially reduced ganglion cell density. The effects of this noise exposure are permanent loss of synaptic ribbons and AN fibers. That this effect occurs in both mice and guinea pigs suggests that it may be common to all mammals (Kujawa and Liberman, 2009; Lin et al., 2011).

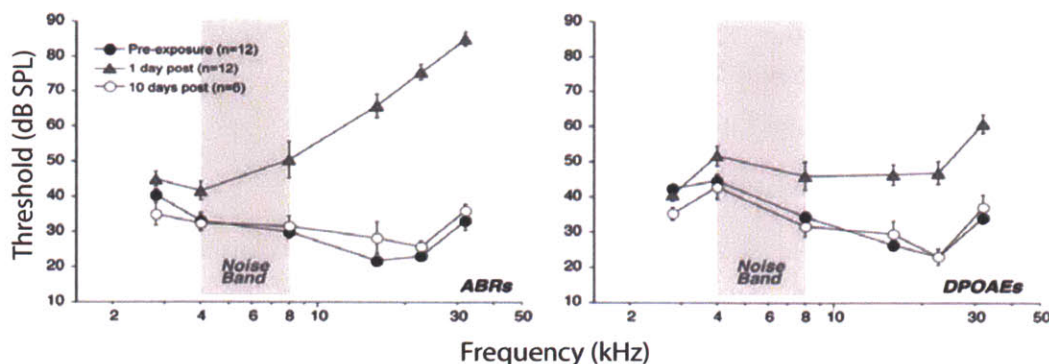


Figure 2 Threshold shift and recovery following 2-hr exposure to 106 dB noise

Guinea pigs exposed to 106dB SPL 4-8 kHz noise suffer large temporary threshold shifts as measured by both ABR (A) and DPOAE (B) responses 1 day post exposure; however, these responses recover to pre-exposure values within 10 days post exposure. The grey shaded area represents the frequency band of the noise exposure. Pre-exposure and 1-day post exposure data are averages from 12 animals and 10 days post exposure from 6 animals. Data

are means and error bars are standard error of the mean. (With permission, from Lin et al., 2011)

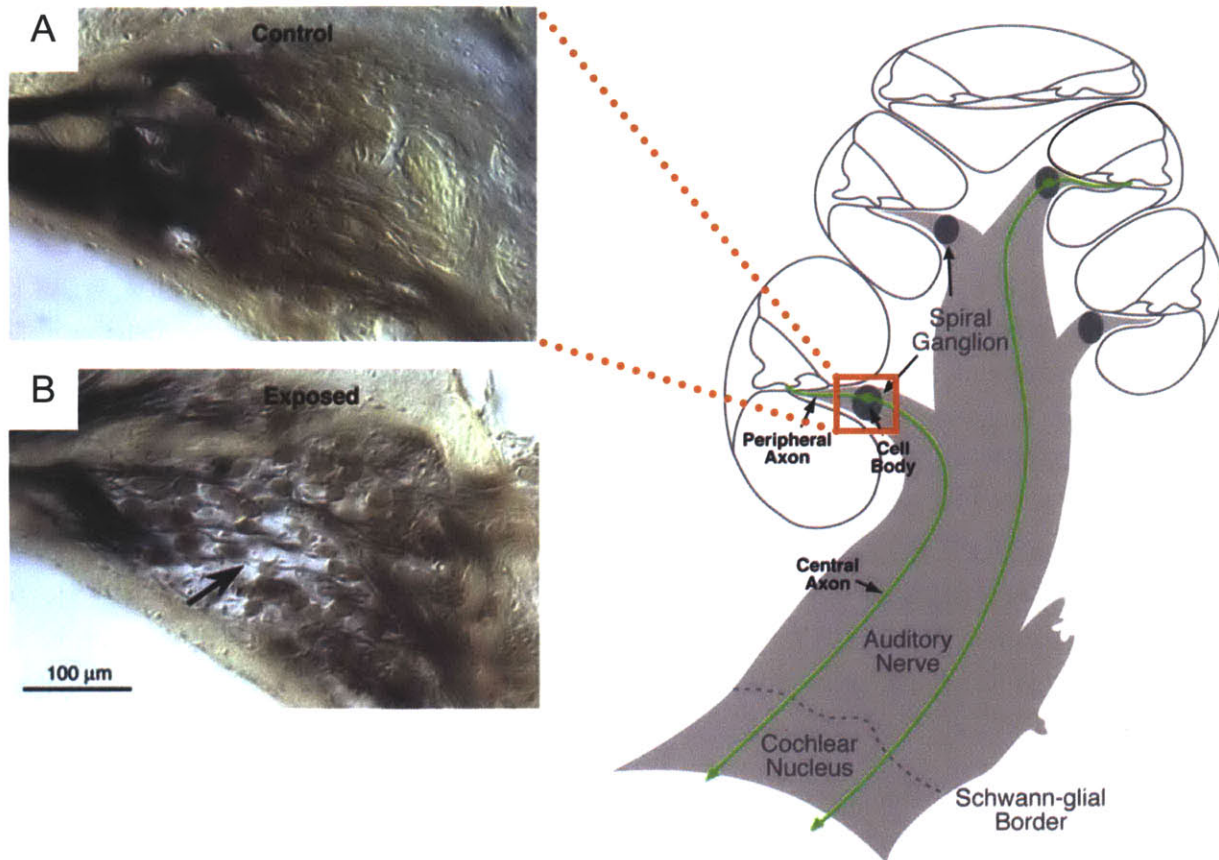


Figure 3 Slow degeneration of spiral ganglion cells after reversible noise-induced threshold shift.

Light micrographs of sections through the spiral ganglion in the basal turn of a control (A) and a (B) guinea pig, 1 yr after exposure to a 106 dB noise for 2 hours., showing the degeneration of spiral ganglion cells. The schematic depicts the anatomical location of the sections. (Data adapted with permission from Lin et al., 2011)

2.3 Single Fiber Recordings and Spontaneous Rate Classifications

The responses of single AN fibers can be measured *in vivo* using glass micropipette-electrodes in an anesthetized animal. The AN trunk is revealed by removing the skull over the cerebellum and retracting the cerebellum, allowing direct access to the nerve. One fundamental aspect of the AN response is the sharp frequency selectivity, which is summarized by tuning curves

which plot the threshold as a function of frequency, i.e. the lowest sound pressure level at which a criterion response rate (e.g. 10 sp/sec over background rate) is evoked (Kiang, 1965). The tip of each tuning curve defines that neuron's characteristic frequency (CF), and the CF, in turn, correlates to where along the cochlear spiral each fiber originates: high-CF fibers synapse on inner hair cells from the cochlear base, low-CF fibers on inner hair cells in the cochlear apex. As shown in Figure 4A thresholds at CF are lowest in the mid frequency region and rise at low- and high-frequency extremes.

The scatterplot in Figure 4A also shows that, at any one CF region, there can be wide range of threshold sensitivity in the normal ear. This threshold range suggests that not all AN fibers are similar. Indeed, AN fibers can also be classified according to their spontaneous firing rate, i.e. the spike rate in the absence of controlled acoustic stimulation. In Figure 4B, the distribution of spontaneous rate is plotted for the same cat as in (A). The fundamentally bimodal nature of the SR distribution suggests that there may be at least two subgroups of AN fibers: those with $SR < 20$ (red) and those with $SR > 20$ (black). As seen in Figure 4A, divided into these two groups, it is clear that low-SR fibers have high thresholds and high-SR fibers have low thresholds. A more careful analysis of the relation between SR and threshold in normal cat AN fibers (Liberman, 1978) suggested it is useful to divide the low-rate group into a low- ($0 < SR < 0.5$ sp/sec) and medium-SR ($0.5 < SR < 20$ sp/sec) subpopulation. That further subdivision of the low-rate group is less clear in guinea pig (Tsuji and Liberman, 1997) and mouse (Taberner and Liberman, 2005).

The full recovery of ABR threshold following sound exposure in the previously mentioned mouse (Kujawa and Liberman, 2009) and guinea pig (Lin et al., 2011) studies suggests that the high-SR fibers may remain but the low-SR fibers may be missing. At threshold levels for the ABR response, the stimulus level is below the response threshold of the low-SR fibers, and as such they do not contribute to measures of ABR threshold. The ABR response at higher stimulus intensities includes a summation of the response from both high and low-SR fibers that are responding to the stimulus. Thus a reduced response to more intense stimuli, when compared to control, could arise from a reduced contribution of the low-SR fibers with no change in the contribution from high-SR fibers.

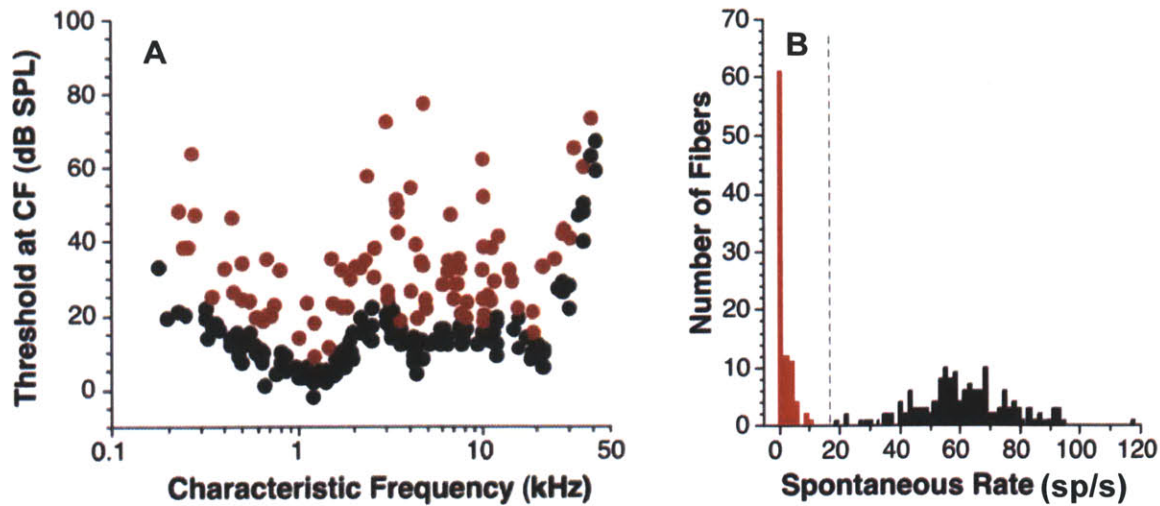


Figure 4 Spontaneous rate and threshold at the CF in single AN fibers

(A) The threshold at characteristic frequency (CF) plotted vs CF for a large number of AN fibers recorded from a single cat. (B) The spontaneous rate (SR) distribution for the fibers plotted in (A). The vertical dashed line separates the High-SR fibers from the Low- and Med-SR fibers. Fibers marked in red in (A) are also red in (B). (Data adapted with permission from Liberman, 1978)

2.4 Synaptic Ribbons and Spontaneous Rate

Additional information about neural losses may be found in the spatial organization of synaptic ribbons around the circumference of the inner hair cell. These ribbons are thought to facilitate the rapid and sustained release of neurotransmitter (Khimich et al., 2005; Nouvian et al., 2006). In the normal ear, ribbons are distributed around the entire basolateral membrane of the inner hair cell, in the subnuclear zone. In the mammalian ear, each IHC afferent synapse has a single synaptic ribbon presynaptic to a single afferent fiber (Liberman, 1980). Low-SR fibers innervate the modiolar side and have large ribbons. High-SR fibers innervate the pillar side and tend to have small ribbons (see Figure 1A). Terminal size and fiber thickness have the opposite trend: low-SR fibers have narrow fibers and small dendritic terminals, high-SR fibers have thick fibers and large dendritic terminals (Liberman, 1982). While exactly how the different morphology contributes to a fibers spontaneous rate is not known, analysis of ribbon organization post exposure could provide another way of looking at the effects of this sound exposure.

2.5 Forward Masking

Among the many AN response properties that systematically differ according to SR, the differences observed in a forward-masking paradigm are particularly relevant to the present study. In forward masking, the response to a stimulus (probe) is decreased by the presence of a

preceding stimulus (masker). This type of masking arises due to depletion of synaptic vesicles by the masker, limiting the amount of vesicles available to respond to the probe. To quantify the effect, the delay between the masker and probe is systematically varied and the time required for the probe response to recover fully (i.e. to equal the response with no masker) is measured (Harris and Dallos, 1979). In gerbil, low-SR fibers recover slowly (>100 ms), while High-SR fibers recover quickly (<100 ms) (Relkin and Doucet, 1991). Relkin et al. (1995) further showed that the differential recovery rates of low vs high-SR fibers could be seen in the recovery of the compound action potential (CAP, which represents the summed activity of the AN) from forward masking. Responses to probe tones presented close to CAP threshold recover linearly in approximately 100 ms. Because these probe tones are below the thresholds of the low-SR fibers, this recovery function must represent the contribution of only the high-SR fibers. However, the recovery functions to more intense probe tones show both a rapid and a slow component with time constants similar to those seen for individual high- and low-SR fibers, respectively. They suggest that the CAP forward masking function could be used to diagnose a selective loss of low-SR fibers: the CAP should recover more quickly from forward masking because the slow contribution from low-SR fibers has been reduced.

Changes to response in a forward masking paradigm could prove useful in a clinical setting by allowing a more precise determination of the pathology underlying a hearing impairment. Selective loss of low-SR fibers may help explain patients that have difficulty hearing in noisy environments but have little threshold shift. Difficulty in noisy environments is a common complaint amongst audiology patients with or without threshold shift (Chung and Mack, 1979; Saunders and Haggard, 1989). If humans with hearing impairment are in fact missing low-SR fibers, then development of an assay could help in clinical hearing assessment and determination of treatment.

3 Specific Aims and Rationale

Aim 1: The first specific aim is to determine the nature of the neuronal loss following a moderate intensity sound exposure that causes no permanent threshold shift in the ABR. This will be done by recording responses of single AN fibers in sound exposed animals, and comparing to responses in unexposed animals. This will test whether there is a systematic loss of low-SR fibers, and whether there are any changes in the response properties of remaining nerve fibers.

Aim 1 Rationale: In our sound exposure model, thresholds are maintained despite loss of neurons and synaptic ribbons. If the loss of neurons were restricted to low-SR fiber types, this would help explain the maintenance of thresholds following noise exposure. Studies have suggested a selective loss of low-SR fibers in aged ears (Schmiedt et al., 1996). We hypothesize that our sound exposure selectively destroys the low-SR fiber population, and that preservation of high-SR fibers is the reason that thresholds are maintained.

Aim 2: The second specific aim is to develop methodology to assay this type of neuronal loss with gross electrophysiology, such as ABR or CAP. By exploiting known differences in the responses of low- and high-SR responses to tone bursts, in a forward masking paradigm, we aim to develop an assay for selective low-SR fiber loss that could ultimately be applied to clinical settings.

Aim 2 Rationale: Low- and high-SR fibers contribute differently to summed neural responses. Using the correct stimulus parameters, the overall contribution of low or high-SR fibers could be assessed and used to infer the numbers of remaining fibers of that type. Relkin (1991) showed that low- and high-SR fibers recover from forward masking at different rates, when masker-induced threshold shift is plotted against the masker-probe interval. At short intervals, the probe response is masked nearly completely, and as the interval gets longer the response recovers to baseline. High-SR fibers are shown to recover in approximately 100 ms, whereas the low-SR fibers can take as long as 1000 ms. They speculate that the CAP forward masking function can be separated into a fast component reflecting the contribution of both low- and high-SR fibers because the time course of recovery for the fast- and slow-components is comparable to the time courses seen at the single fiber level. We hypothesize that loss of low-SR fibers will cause the CAP to recover more quickly from forward masking than when the low-SR fibers are still intact.

Aim 3: The third specific aim is to evaluate the synaptic changes in the inner hair cell area histologically. Low-SR fibers predominately contact the modiolar side of the hair cells and high-SR fibers contact the pillar side of the hair cell. There exist gradients of ribbon size and

terminal size that also parallel differences in spontaneous rate. Staining for presynaptic ribbons and postsynaptic receptors may help interpret patterns of neural degeneration.

Aim 3 Rationale: There are several morphological gradients in the cochlea related to spontaneous rate. Low-SR neurons have thinner dendritic fibers and smaller terminal endings than high-SR neurons. There is spatial segregation of low- vs. high-SR neurons, where the low-SR fibers tend to innervate the modiolar side of the hair cell and the high-SR fibers the pillar side of the hair cell (Liberman, 1982). Low-SR neurons tend to have larger synaptic ribbons than their high-SR counterparts (Liberman, 1980, 1982). We hypothesize that the pattern of ribbon loss will reflect loss of low-SR suggested in Aim 1.

4 Methods

4.1 Animals and Groups

All animals used in this project were female, white albino Hartley Guinea Pigs. They arrived at 1 month of age and had body weight approximately 250g. Animals were housed in the MEEI animal care facility and testing was completed within two months of arrival. Some animals were sound exposed and then allowed to recover. Others served as non-exposed controls and were housed in the same cage as their sound exposed counterparts. All procedures were approved by the Institutional Animal Care and Use Committee at the Massachusetts Eye and Ear Infirmary.

Single-fiber data was collected in 15 control guinea pigs, and 9 exposed guinea pigs. CAP forward masking data were obtained from an additional 3 control and 4 exposed animals where no single fiber results were obtained. ABR and DPOAE recovery data presented are from the 9 exposed guinea pigs that generated the noise-exposed single fiber data.

Animals were sacrificed at the end of single fiber or CAP recordings, and tissue was processed for confocal microscopy. Eleven exposed and 4 control animals were immunostained with antibodies against CtBP2 to allow counts of synaptic ribbons, and all of these animals were included in the single-fiber data. A subset of these ears was processed to analyze GluR2 and CtBP2 staining. Both ears from 3 exposed and 1 control guinea pig were used. These ears were used for ribbon volume analysis, GluR2 patch volume analysis, and ribbon-GluR2 pairing analysis. Data from the left ear of all 4 of these animals contributed to the single fiber dataset.

4.2 Noise Exposure

For noise exposure (to a 4-8 kHz octave-band noise at 106 dB SPL for 2 hrs), animals were awake and unrestrained in a cage on a rotating platform inside of an acoustically reverberant wooden chamber. The sound source was a compression driver (JBL Model 2446H) attached to an acoustic horn, driven by a power amplifier (Crown Power Amplifier D75A). A computer running custom LabView software delivered the stimulus and monitored the output via a B&K ¼" Condenser Microphone, calibrated against a B&K Pistonphone. Animals were allowed to recover for two weeks post exposure. This recovery time allows thresholds to recover to normal, which was assessed via ABR and DPOAE recordings prior to recording from the auditory nerve.

4.3 ABR and DPOAE Measures

Cochlear function was assessed using ABR and DPOAE responses while the animal was anesthetized with a combination of nebutal (25mg/kg, I.P.), fentanyl (0.15mg/kg, I.M.) and

droperidol (7.5mg/kg, I.M.). Animals were allowed to recover from anesthesia after recording ABR and DPOAE, and then returned to the animal care facility. Exposed animals were tested twice, once prior to exposure, and once 14-days after exposure.

All *in vivo* recordings used the same custom acoustic assembly designed in-house by the engineering staff at EPL. This assembly uses two earphones to deliver sound to the ear canal and an electret condenser microphone (Knowles FG-23329-P07) coupled to a probe tube to measure sound pressure level at the output port of the system. The acoustic assembly was not sealed to the ear canal, however care was taken to always position the assembly in a similar fashion. Probe microphone responses were amplified and passed to the analog-to-digital I/O board. Sound pressure level was measured as a function of frequency with the probe tube microphone every time the acoustic assembly was placed at the ear canal. All recordings were made in an acoustically and electrically shielded, double walled chamber, heated to 92 F.

ABRs were measured using custom LabView software to generate stimuli and record the responses. Needle electrodes were placed subcutaneously at the pinna, the vertex of the skull, and a reference ground in skin of the lower back. Stimuli were 4.0 ms tone pips, with a 0.5 ms rise/fall delivered at a rate of 40/sec. Stimulus polarity was alternated to allow removal of microphonic potentials. Responses were averaged to 512 tone-pip pairs. Tone pip frequency was varied from 2.83 to 45.25 kHz in half-octave steps, and stimulus level was varied from 10 to 80 dB SPL in 5 dB steps. This allowed for the detection of ABR threshold, as well as evaluation of the entire amplitude vs. level function at that frequency. ABR threshold was measured by visual inspection of stacked waveforms.

DPOAEs were also measured using custom LabView software. DPOAE stimuli were two pure tones (f_2 and f_1) in a frequency ratio of $f_2/f_1 = 1.2$ and at a level ratio of $L_1 = L_2 + 10$ dB. Each speaker in the acoustic assembly was driven with only a single pure tone to limit distortion from the acoustic system itself. DPOAE response was measured as the amplitude of the $2f_1-f_2$ peak following FFT analysis of the averaged probe tube microphone response. Both waveform and spectral averaging were used. DPOAE threshold was defined as the interpolated primary level (of f_2) required to produce a DPOAE amplitude of 0 dB SPL.

4.4 Anesthesia and Surgical Preparation for Single Fiber and CAP Recordings

Animals were deeply anesthetized with a combination of urethane (900 mg/kg, I.P.), fentanyl (0.15 mg/kg, I.M.), and droperidol (7.5 mg/kg, I.M.). Surgery was performed in the acoustically and electrically shielded chamber that was kept at 92 F, and a supplemental heating pad was used as necessary to maintain body temperature around 100 F. Once a surgical plane of anesthesia was reached, animals were mounted to a headholder with a bite bar and dental cement, and the pinnae were reflected bilaterally. Ear canals were severed as close as possible

to the skull, and all surrounding blood vessels were carefully cauterized. Muscle tissue was removed from the bulla as well as the back of the skull. The bulla was opened, and a silver wire was placed in a bony niche close to the round window membrane to measure the CAP via a Grass amplifier. The CAP response to a low-level click was monitored during subsequent surgery to ensure that cochlear sensitivity remained stable. The back of the skull was opened using rongeurs. The area was cleaned of any bleeding or residual blood by rinsing with cold (40°F) physiological saline (0.9 % NaCl in distilled water) which also aided in clotting. The dura covering the exposed portion of the brain was resected, and the left portion of the cerebellum and the floccular lobe were aspirated exposing the cochlear nucleus. All exposed portions of the brain were covered with a thin layer of fluffed cotton. Several pieces of cotton were rolled into very small balls by hand, and placed anterior to the cochlear nucleus. Posterior to the cochlear nucleus a small tube-shaped roll of cotton was placed. The cotton helped to reduce motion of the auditory nerve from pulsation of the brain due to breathing or the heartbeat. It additionally provided a means to remove fluid around the nerve, necessary for completing the surgery and visually guiding placement of the recording electrode. The last step was to gently move the cochlear nucleus medial and slightly rostral, so that to the AN trunk within the internal auditory meatus could be visualized. An extra piece of cotton was placed between the tip of a curved copper retractor attached to a ball-joint manipulator (Narishige, Japan). This manipulator allowed for precise, controlled motion of the retractor, as it is very easy to damage the cochlear nucleus or the AN if any of it is moved too far. Damage would be immediately visible in the CAP click response. Because of the invasive nature of this surgery, cochlear sensitivity tended to degrade with time over the course of an experiment. CAP thresholds were monitored regularly, and the experiment was terminated when thresholds had shifted more than +10 dB over half of the cochlea, i.e. for all frequencies above or all frequencies below 16 kHz, although the tendency was to lose high-frequency sensitivity first.

4.5 CAP Thresholds and Forward Masking Functions

The CAP thresholds and forward masking functions were recorded following surgical access to the round window membrane, but before surgical preparation for the single-fiber experiments. Stimuli were generated by custom Labview software and delivered through the same acoustic assembly. Responses were recorded through the silver wire, which was connected through a Grass amplifier and processed by the custom LabVIEW software. CAP thresholds was measured under computer control with an algorithm that tracks the SPL required to produce a response (average of 16 stimulus presentations) of 15 μ V peak-peak in response to 4 ms tone pips with a 0.5ms rise/fall presented at a rate of 10/s. Forward masking stimuli were a 100 ms tonal masker followed by a 5 ms probe, 0.5 ms rise/fall. Both probe and masker were at 17.54 kHz, at a level 40 dB above the CAP threshold at that frequency. The frequency was chosen to be in the middle of the cochlear region where noise-induced synaptic degeneration was maximal

(and also at a precise frequency that happened to be tested by the CAP threshold tracking software). Stimuli were presented at an overall rate of 1.5/s and responses were averaged 32 times at each masker probe interval, which was varied from 8 to 1024 ms in octave steps.

4.6 Recording of Single Fibers

Single-fiber responses were recorded using glass micropipettes (World Precision Instruments, Borosil 1.2mm OD x 0.9mm ID #30-31-0) that were pulled to a very fine tip using an electronically controlled electrode puller (Flaming-brown P80/pc). Electrode quality was evaluated visually with a light microscope (Leitz Ortholux with Zeiss Neofluor 40x objective). Impedance was not routinely measured, but averaged between 10-30 M Ω . Electrodes were filled with 2M KCl and mounted in a half-cell electrode holder (MEH3s12, WPI) and advanced remotely using a remotely controlled hydraulic Microdrive (Kopf 607C, David Kopf Instruments). Spikes were amplified using a low-noise battery-powered amplifier (Ithaco Model 1201), and then passed to the computer for analysis. A broadband noise burst (70-80 dB SPL) was used as search stimulus while advancing the electrode.

Once a neuron was isolated, several response properties were measured. The first response property measured was always the spontaneous activity, i.e. the average rate over 30 sec in the absence of controlled acoustic stimulation. The tuning curve, measured next, represents an isorate contour (10 spikes/sec > SR) in response to 50-ms tone bursts (2.5 msec rise-fall) presented (10/sec) over a range of frequencies (Kiang et al., 1970). The tip of this tuning curve provided the characteristic frequency (CF) and threshold at CF of that fiber.

A post stimulus time histogram (PSTH) was recorded in response to 200 presentations of a 50 ms tone burst presented 30 dB above threshold at the CF. A rate-level function was recorded by presenting 50 msec tone bursts at CF over a range of stimulus levels (0 to 80 dB SPL, 50 presentations per level, presented in random level order). Rate-level functions were fit using a model published previously (Taberner and Liberman, 2005), which provided a measure of the fiber's dynamic range, defined as the difference in stimulus SPL required to drive the neurons from 10% to 90% of the maximum discharge rate.

Forward masking was tested in a subset of AN fibers. The stimuli were a 100ms masker presented at CF, 40 dB above threshold, followed by a 15 ms probe tone also at CF and also presented 40 dB above threshold. The delay between the masker and the probe (the masker-probe interval) was varied from 2 to 256 ms in logarithmically spaced steps, and averaged 25-50 times at each interval. The PSTH for each interval binned in 1 ms increments and analyzed for the peak response to masker and to probe. Data was normalized to the masker response as "Normalized Decrement." The normalized decrement curves were fit with a linear function of

delay on a log axis, which provided an estimate of the masker-probe interval required for that fiber to recover fully.

4.7 Histological Analysis

We histologically examined cochleas from control and noise-exposed guinea pigs to evaluate the numbers, sizes and spatial organization of pre-synaptic ribbons and post-synaptic glutamate receptors. After fixation, decalcification and dissection, organ of Corti cochlear whole mounts were immunostained for some combination of the following markers: CtBP2, which stains synaptic ribbons, Na^+/K^+ ATPase (NKA), which stains the peripheral unmyelinated terminals of AN fibers, myosin-VIIa, which stains inner and outer hair cells, and GluR2, which stains the post-synaptic AMPA-receptor patches on AN fibers. Confocal z-stacks through the entire synaptic zones of 7-9 adjacent IHCs were then acquired at regularly spaced intervals along the cochlear spiral.

4.7.1 Tissue Fixation

At the conclusion of a terminal experiment, some animals were exsanguinated and perfused intracardially to prepare tissue for histological analysis. Animals were overdosed with pentobarbital (117 mg/kg, I.P.), then perfused intracardially with saline (154 mM NaCl and 14.5 mM NaNO_2) for approximately 60 sec or until discharge fluid started to run clear, then perfused with 4% paraformaldehyde for 5 minutes. After perfusion, both cochleae were removed, the round and oval windows were opened, and fixative was gently applied to both openings with a small syringe. Cochleae were then postfixed for varying times, according to the type of immunostaining. Ears stained for CtBP2, NKA and myosin were fixed overnight at 40°F. Ears stained for CtBP2, GluR2 and Myosin were fixed for 1 hour at room temperature on a shaker table (VWR Orbital Shaker). Cochleae were then allowed to decalcify for approximately 3 weeks in a solution of EDTA (120mM, pH 7.0) at room temperature on a shaker table.

4.7.2 Microdissection and Immunological Staining

The organ of Corti was micro-dissected into approximately 11 pieces, and one of two immunostaining protocols was utilized.

a) CtBP2-NKA α 3-MyosinVIIa: Tissue was permeabilized by immersion in 30% sucrose for 20 min on a shaker table, freezing on dry ice, then thawing and treatment in a PBS rinse for 20 min on the shaker table. Tissue was blocked for one hour on the shaker table in 5% NHS with 1% triton, then incubated overnight at 37°C in primary antibodies. Primary antibodies were mouse-anti-CtBP2 (1:50, BD Transduction Labs, #612044), goat anti-NKA α 3 (1:100, Sant Cruz, #sc-16052) and rabbit anti-myosinVIIa (1:100, Proteus BioSciences, #25-6790). Tissue was rinsed in PBS three times over 10 min, and then incubated for one hour at 37°C for secondary antibody attachment: Biotinylated donkey anti-mouse (1:200, Jackson ImmunoResearch, #7115-065-

150), AlexaFluor488 chicken anti-goat (1:1000, Invitrogen, #A21467), and donkey anti-rabbit-AF647 (1:200, Invitrogen, #A31573). Tissue was rinsed and then incubated for another hour at 37°C in another set of secondary antibodies: Streptavidin-conjugated AlexaFluor568 (1:1000, Invitrogen, #S11226), AlexaFluor488 goat anti-chicken (1:1000, Invitrogen, #A11039), and donkey anti-rabbit-AF647 (1:200, Invitrogen, #A31573). Tissue was rinsed, mounted and coverslipped with Vectashield (Vector Labs, #H-1000).

b) CtBP2-GluR2-MyosinVIIa: Tissue was permeabilized and blocked as above. Primary antibody was applied in an overnight incubation at 37°C: mouse(IgG1) anti-CtBP2 (1:50, BD Transduction Labs, #612044), mouse(IgG2a) anti-GluR2 (1:1000, Millipore, #MAB397), and rabbit anti-myosinVIIa (1:100, Proteus BioSciences, #25-6790). Tissue was rinsed three times in PBS, then incubated for two hours at 37°C in secondary antibodies: goat anti-mouse (IgG1) AlexaFluor568 (1:500, Invitrogen, #A21124), goat anti-mouse (IgG2a) AlexaFluor488 (1:500, Invitrogen, #A21131), and donkey anti-rabbit AlexaFluor 647 (1:200, Invitrogen, #A31573). Tissue was rinsed, mounted, and coverslipped in VectaShield (Vector Labs, #H-1000).

4.7.3 Microscopy and Image Analysis

Cochlear Mapping

Slides were first imaged in an epi-fluorescence microscope (Nikon Eclipse E800) to map cochlear frequencies to dissected pieces in each case. Digital images, captured using a Microfire Optronics camera and a 4x objective (Nikon Planapochromat), were compiled into a montage using ImageJ (NIH). A custom ImageJ script was used (<http://www.masseyeandear.org/research/ent/eaton-peabody/epl-histology-resources/>) in which the user traces the arc of the inner spiral bundle in each dissected piece of the organ of Corti. This script produces a spline fit to the user-generated arc, measures the relative positions along the spiral and applies a physiological place-frequency map for the guinea pig (Tsuji and Liberman, 1997) to overlay frequencies onto the montage image of all the dissected pieces. This cochlear “roadmap” allows us to acquire confocal data at precisely place-matched regions of the organ of Corti in each case.

Confocal microscopy

IHC synaptic zones were imaged at 6 log-spaced frequency locations (2, 4, 8, 16, 32 and 45 kHz) on a Leica SP2 confocal. Images were captured with a 100x oil immersion objective (N.A. 1.4), and a 2x digital zoom. Two adjacent images were captured at each frequency location. Fluorofluors were excited with three lasers at 488nm, 568nm, and 647nm. All three channels were excited simultaneously as the computer captured z-slices (spaced at 0.2442 um) of the IHC region. This usually encompassed approximately 8 IHCs per image stack.

Confocal images were analyzed offline using Amira (Visage Imaging). For every set of images, pre-synaptic ribbons and glutamate receptor patches were counted, and their volumes estimated, using the “connected components” tool in Amira. This tool takes a user-specified pixel-intensity criterion and identifies, for the selected channel (R,G or B), all the voxel spaces within which all the pixels meet or exceed the criterion intensity. By then displaying each of these connected components as a surface contour superimposed on, for example, the maximum projection in the same channel, the user can easily see if the criterion selected does a good job of exactly capturing the elements of interest, e.g. synaptic ribbons. The Amira output provides the total number of elements, each element’s xyz coordinates and each element’s volume. Further analysis of the Amira output data was carried out in Matlab (Mathworks) and Microsoft Excel. Ribbons and glutamate receptor patches were analyzed for their modiolar-pillar location within the IHC and for changes in volume. Pairing of pre- and post-synaptic markers was evaluated by generating a series of high-power thumbnail images, each centered at the xyz positions captured in Amira. These thumbnails allowed for easy identification of ribbons missing a juxtaposed receptor patch, and of receptor patches missing a juxtaposed synaptic ribbon.

5 Results

5.1 Noise Exposure and Cochlear Function

Prior work (Lin et al., 2011) showed that, for a noise band at 4-8 kHz (roughly in the middle of the guinea pig's hearing range) and a duration of 2 hrs, an intensity of 106 dB SPL represented the highest level for which thresholds would return to pre-exposure levels within 1-2 wks. Thus, this exposure is near the borderline between reversible and irreversible threshold shift.

5.1.1 ABR and DPOAE Recovery

Each animal's cochlear function was tested prior to and 14 days after the noise exposure using both ABR and DPOAE metrics. Whereas ABR wave-1 provides a measure of the ensemble neural output of the cochlea including all elements of the mechanoelectric transduction and synaptic transmission cascade, the DPOAE responses can be used to assess the "pre-synaptic" elements "upstream" of the inner hair cells and their synapses with cochlear nerve fibers (Liberman et al., 1997). DPOAEs are dependent on proper functioning of the middle ear, the OHC amplifier, and a sufficient endocochlear potential (Lonsbury-Martin and Martin, 1990). DPOAEs are generated by the mechanical interaction of two pure tones when amplified by the active processes in the OHCs. These distortion products occur at intermodulation frequencies of the form $nf_1 - mf_2$, and are passed back out of the cochlea through the middle ear and into the ear canal. A sensitive microphone can detect the amplitude of these distortion components; the $2f_1 - f_2$ frequency was measured in these studies.

As shown in Figure 2, prior study demonstrated that the exposure to 4-8 kHz noise band at 106 dB for 2 hrs causes up to 50 dB of acute threshold shift, when measured 24 hrs after exposure (Lin et al., 2011). By 2 wks after exposure to the same noise band, DPOAE thresholds in the present study were within 5 dB of pre-exposure levels (Figure 5A,B), and some of the small pre/post differences in mean threshold were in the direction of response enhancements. The DPOAE amplitude-vs-level functions also showed a complete return to pre-exposure levels (Figure 5C,D), suggesting normal OHC function regardless of stimulus level.

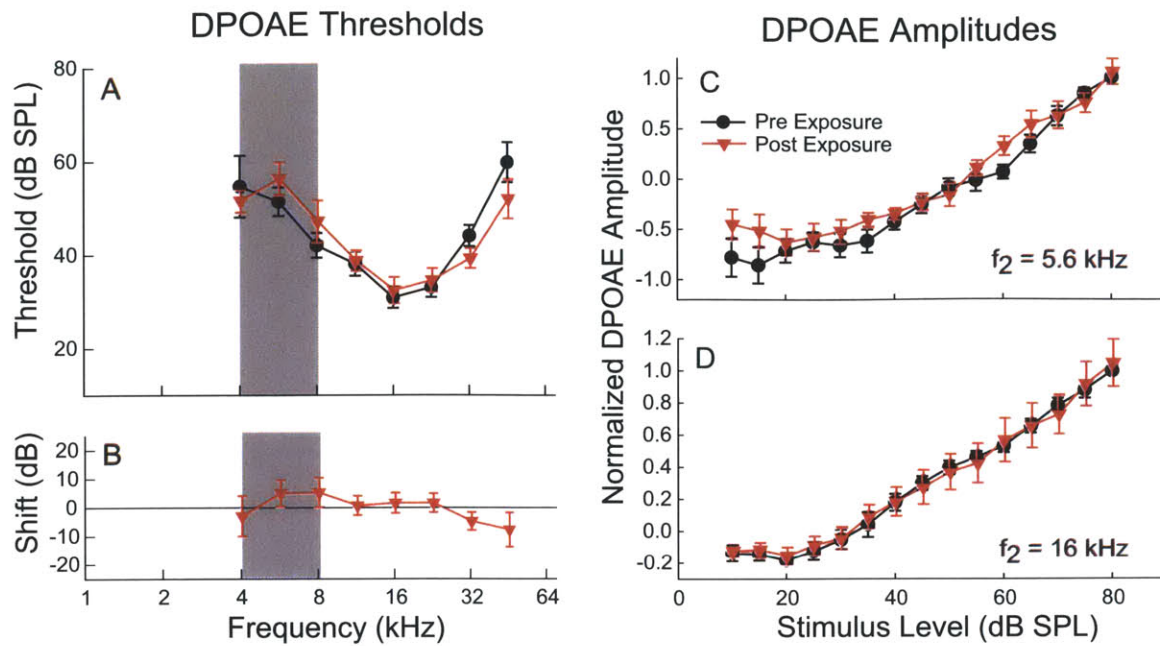


Figure 5 DPOAE thresholds and suprathreshold amplitudes recover after exposure to the 106 dB noise band

(A) Mean DPOAE responses from 9 guinea pigs, each measured pre and post exposure. (B) Threshold shifts (post-exposure minus pre-exposure) were less than 5 dB at all frequencies. (C,D) DPOAE amplitudes to suprathreshold tones also fully recover to pre-exposure levels, shown for $f_2=5.66 \text{ kHz}$ (C) and 16 kHz (D). All points are group means (\pm SEMs). Differences between groups are not statistically significant (ANOVA, $P \gg 0.01$).

The ABR is recorded differentially across two needle electrodes that span the cochlea: one outside the pinna and one at the vertex of the skull. The ABR wave represents the summed neural activity that is synchronized to the acoustic stimulus. The different peaks, or waves, of the ABR response reflect the activity of different portions of the ascending auditory pathway. Wave-1 is predominately the activity in the auditory nerve, while later waves are influenced by activity from other areas of the ascending auditory system. ABR threshold was considered as the lowest intensity where any ABR wave could be identified, giving us a threshold resolution of 5 dB. Most commonly, it was only wave-3 that appeared at the intensities near threshold. Figure 6A shows ABR threshold recovery as absolute threshold, and Figure 6B shows the ABR threshold shift 2 wks after exposure. ABR threshold shift was approximately 5 dB at 4 and 6 kHz, with a maximum of 10 dB at 8 kHz. Thresholds were similar or better than pre-exposure values at all other frequencies.

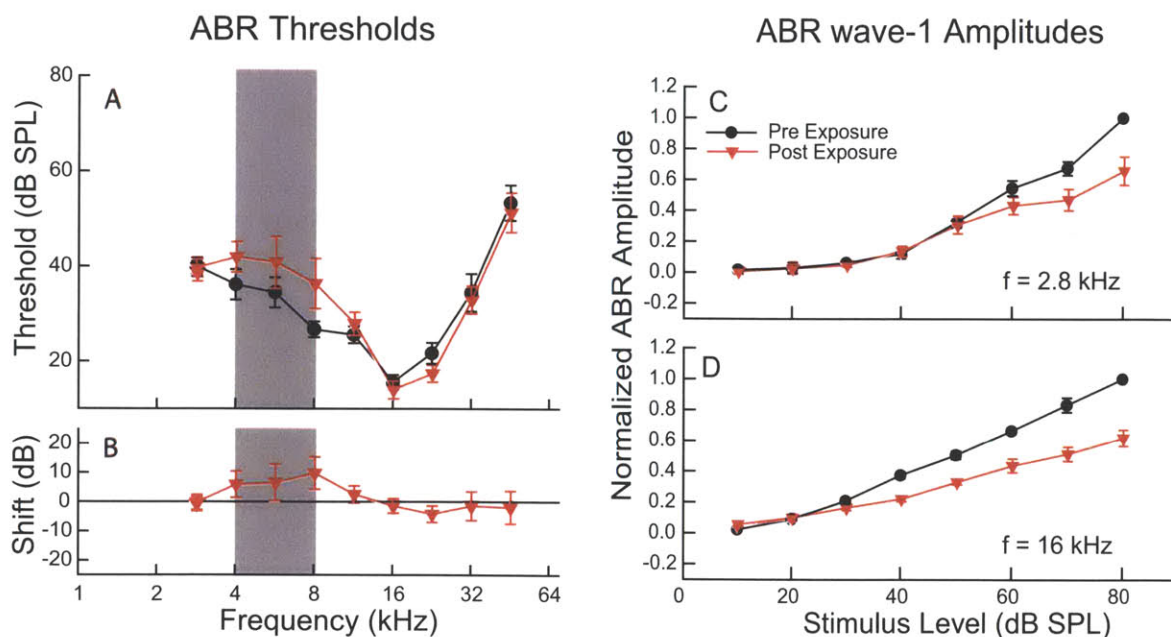


Figure 6 ABR thresholds recover at high frequencies after exposure, but wave-1 amplitudes do not

(A) Mean ABR Threshold as a function of frequency for the same 9 guinea pigs as Figure 5. (B) ABR threshold shift (post-exposure minus pre-exposure) as a function of frequency. Inter-group threshold differences are not statistically significant (ANOVA, $P > 0.01$) (C) The amplitude of ABR wave-1 peak grows with stimulus intensity, and largely recovers at frequencies below the sound exposure. At 2.8 kHz, post exposure responses are significantly reduced only at 70 and 80 dB (ANOVA, $P < 0.05$). (D) At 16 kHz, the amplitude of ABR wave-1 does not recover to pre-exposure magnitude. Post exposure responses are significantly

reduced for stimulus intensities over 40 dB SPL (ANOVA, $P < 0.01$). Data for (C, D) are normalized to the 80 dB SPL pre-exposure peak response for each animal. All points are group means (\pm SEMs).

5.1.2 Reduced ABR Wave-1

As stimulus intensity is increased, the amplitude of the ABR increases because higher intensity sounds recruit activity from more neurons and cause responding neurons to fire action potentials at an increased rate. The growth of any ABR wave amplitude can be plotted against stimulus intensity to provide an ABR I/O function. Following noise exposure, the ABR I/O functions did not recover despite the recovery of threshold. Figure 6D shows the average ABR wave-1 amplitude at 16 kHz, plotted against stimulus intensity. Functions were normalized to the pre-exposure responses at 80 dB SPL. These data reflect a 47% decrease in the 16 kHz ABR response at 80 dB SPL. Post-exposure reduction in amplitude at 16 kHz was statistically significant for intensities over 40 dB SPL (ANOVA Pairwise Comparison, $P < 0.01$). This “ABR Wave 1 Phenotype” parallels that seen in mice (Kujawa and Liberman, 2009) exposed to a mid-frequency noise band for 2 hrs, at a level titrated to be at the border between reversible and irreversible threshold shift. Figure 6C shows the average ABR wave-1 amplitude at 2.83 kHz, a frequency below the exposure band. These responses fully recover except at the intensities above 60 dB SPL; the differences are statistically significant only at 70-80 dB SPL (ANOVA Pairwise Comparison, $P < 0.01$) where responses from high-frequency regions with synaptic losses (See section 5.4.3) are likely contributing to the ABR.

5.2 Single Fiber Responses

Recording the response properties of single fibers is an invaluable way to assess the functioning of the AN. Seminal work in the 1960's from the Kiang laboratory laid the groundwork for this technique (Kiang, 1965). Since prior work (Kujawa and Liberman, 2009; Lin et al., 2011) shows that there is neuronal loss following this sound exposure, close examination of AN responses was used to infer which neurons were lost and the normality of remaining neurons.

5.2.1 Tuning Curves and Spontaneous Rate

Fibers were first classified by recording spontaneous activity. Spontaneous activity was measured as the average firing rate during a 30 s period of silence. Next, the tuning curve was measured by a computer-driven algorithm that tracks the iso-response contour representing 10 spikes/sec over spontaneous rate. Some example tuning curves can be seen in Figure 7. The tip of the tuning curve defines a fiber's characteristic frequency (CF), as well as its threshold at CF, the lowest intensity-frequency combination to which the AN responds. The control and exposed fibers in Figure 7 were chosen because they had similar thresholds at CF. Tuning curves from exposed ears do not appear to differ substantially from those measured in unexposed controls.

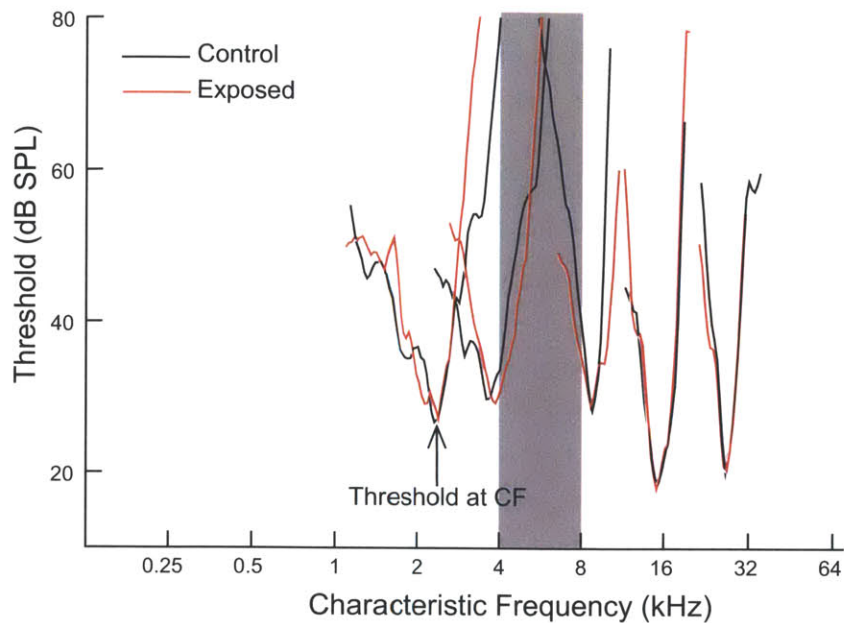


Figure 7 AN Tuning curves appear unchanged post exposure

Ten representative tuning curves from control and exposed ears were selected by choosing fibers with closely matched CFs and thresholds at CF.

5.2.2 Thresholds at CF

With a large database of control and exposed AN fibers, we can evaluate various metrics throughout the fiber populations. One highly informative way to summarize the results is to plot the distribution of thresholds at CF, coded for spontaneous rate (SR), with SR groups defined as in prior study (Tsuji and Liberman, 1997). In Figure 8 we plot the threshold distribution for control fibers (A), and the distribution of exposed fibers (B). As expected, control responses resemble those seen in other studies of the vertebrate AN (Kiang, 1965; Liberman, 1978; Taberner and Liberman, 2005; Furman et al., 2006): i.e., high-SR fibers tend to have the lowest thresholds, medium-SR fibers have intermediate thresholds, and the low-SR fibers have the highest thresholds.

In the exposed ears, the numbers of low- and medium-SR fibers seem reduced in the basal half of the cochlea, however the CF-thresholds of remaining medium- and low-SR fibers appear normal. The relatively high thresholds of some of the high-SR fibers between 4 and 8 kHz may

represent some permanent noise-induced threshold shift in a couple of animals (See Figure 6A,B). This threshold shift is not seen in the mean CAP threshold functions measured 2 wks post exposure (Figure 9) however there existed a large amount of inter-animal variability in that frequency region as seen by the large standard errors. CAP threshold data represent the means from all control and exposed animals included in Figure 8. Note that CAP thresholds, as measured here, are systematically higher than ABR thresholds (Figure 6). This is partially due to differences in the amount of averaging (16) and the choice of threshold criterion (15 μ V). Additionally, CAP threshold more directly reflects activity in the AN, whereas ABR threshold is determined by lowest intensity to produce a detectable ABR wave after 512 averages, often wave-3.

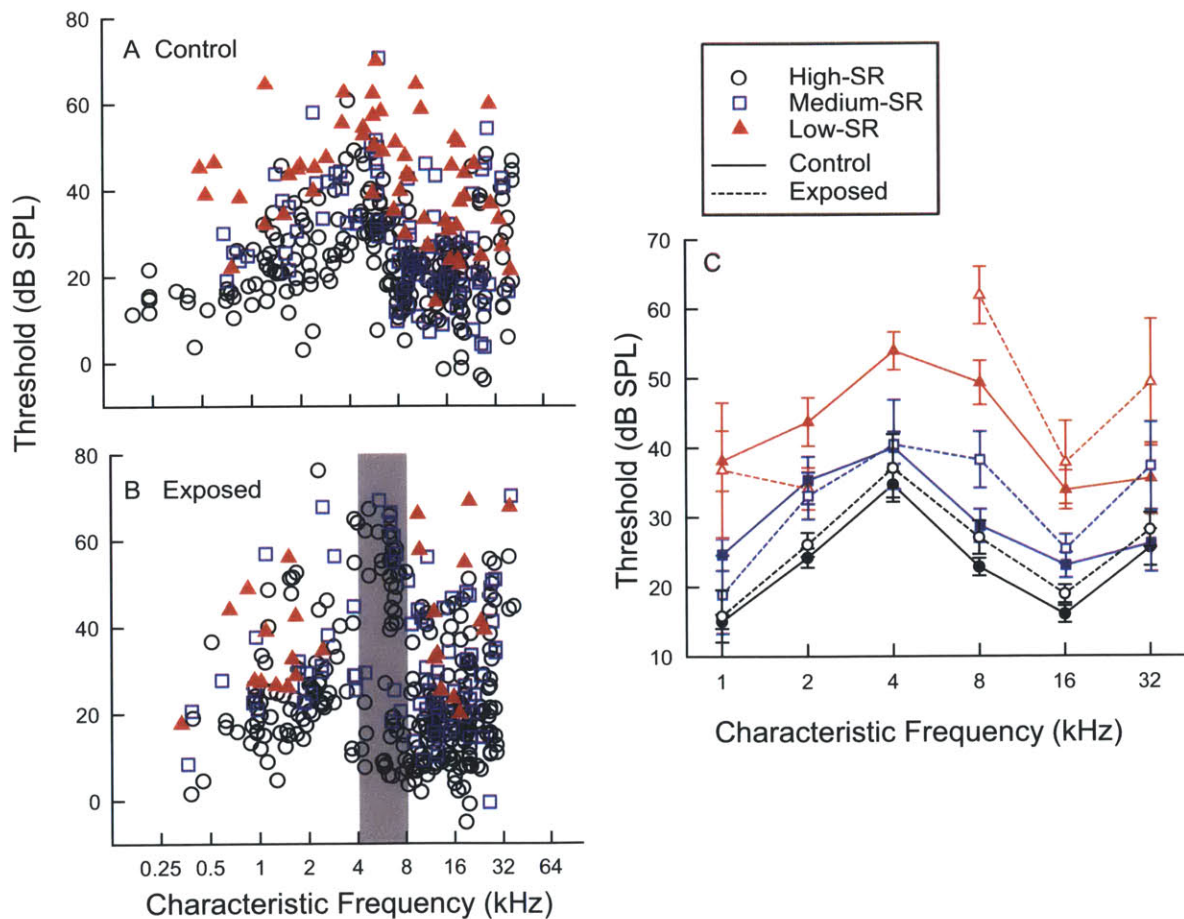


Figure 8 Thresholds at CF vs CF for control and exposed ears

The threshold at CF is plotted for control (A) and exposed ears (B). Each fiber is coded for its SR: high-SR in black circles, med-SR in blue squares, and low-SR fibers in red triangles (See Tsuji and Liberman (1997) for SR group criteria). Control n = 367 fibers from 14 animals, Exposed n = 382 from 9 animals. (C) Group means and standard errors of the mean plotted against CF. Differences between control and exposed within SR-type groups are not statistically significant (ANOVA, $P > 0.05$).

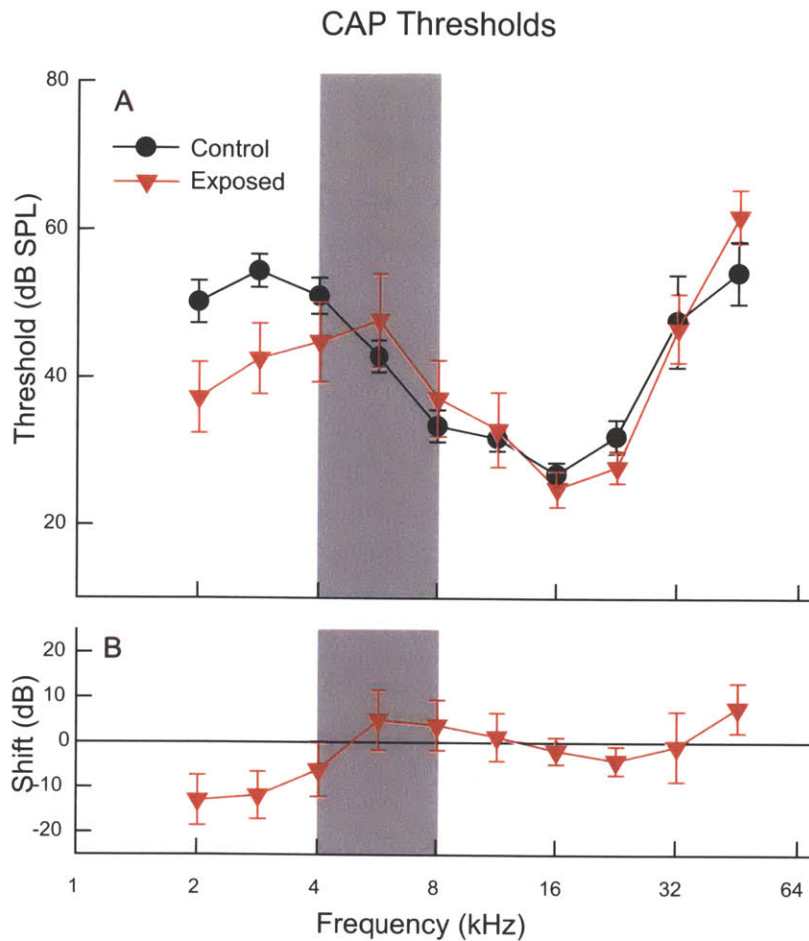


Figure 9 Mean CAP thresholds are normal post-exposure

The CAP threshold (A) is plotted against frequency for the same ears as in Figure 8. Threshold was defined as a CAP response that exceeded 15 μ V peak-to-peak in response to 16 presentations of a 5 ms tone pip. (B) Threshold difference in the CAP: exposed minus control. All points are group means (\pm SEMs). Differences between groups are not statistically significant (ANOVA, $P > 0.05$) except at 5.6 kHz (ANOVA Pairwise Comparison, $P < 0.05$).

5.2.3 Spontaneous Rate Distributions

In order to quantify the apparent loss of low- and med-SR fibers, we plot the distribution of SR separately for low and high frequency halves of the cochlea. In the apical half of the cochlea (CF < 4 kHz), where noise exposure effects should be minimal, the distribution of SR post exposure is similar to that seen in unexposed controls and the differences between distributions

were not statistically significant ($P > 0.05$ by Kolmogorov-Smirnov). On the other hand, in the basal half of the cochlea, ($CF > 4$ kHz) the low- and med-SR fibers comprise 47% of the total population in control ears vs 29% in the exposed ears. This represents a relative loss of low-SR fibers by about 38%. For $CFs > 4$ kHz, there was a highly significant difference between the control and exposed distributions (Kolmogorov-Smirnov, $p \ll 0.01$).

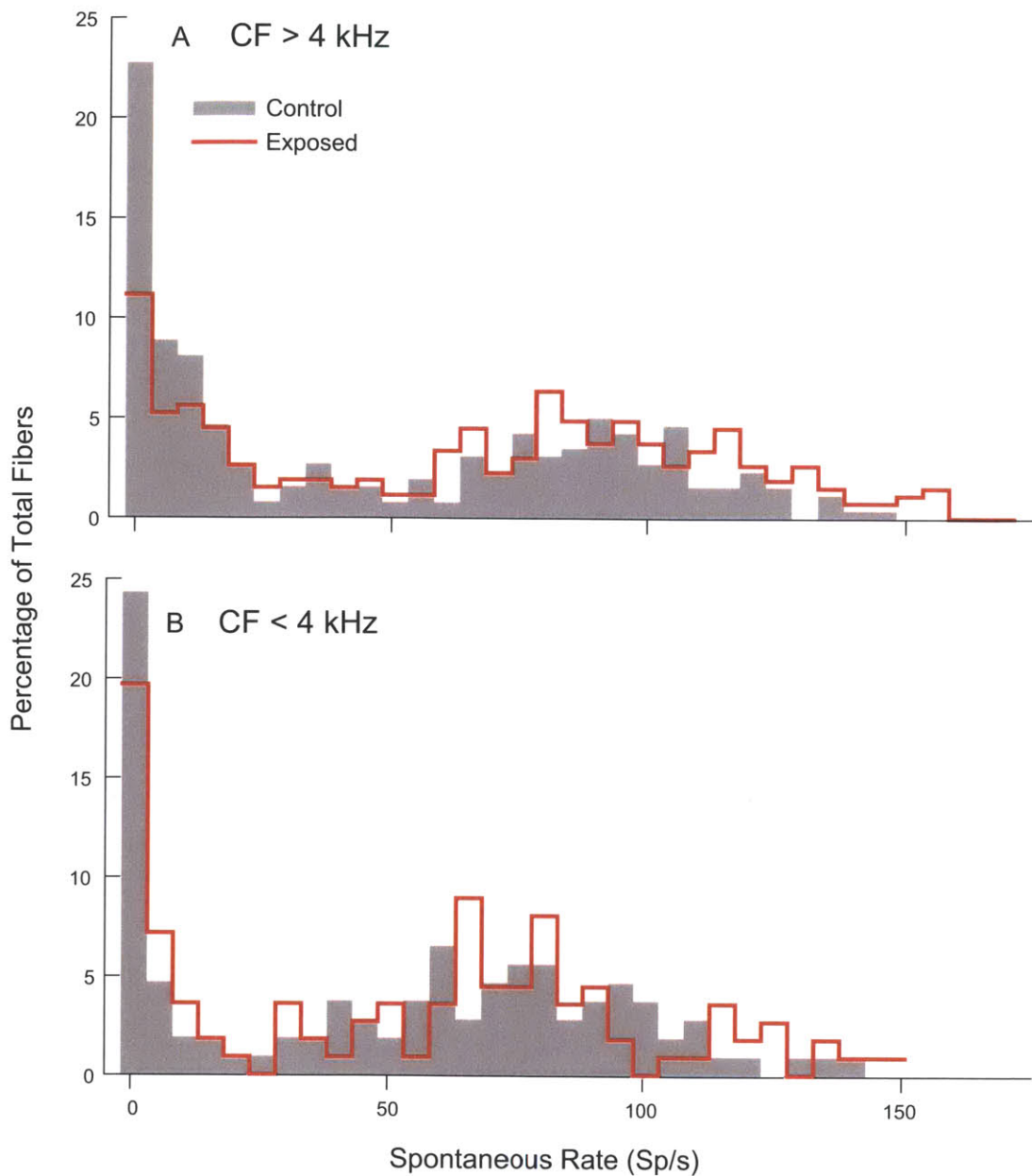


Figure 10 Spontaneous rate distributions suggest a selective loss of low-SR fibers in the basal half of the cochlea

SR distribution plotted as percentage of total fibers for (A) all fibers with CF over 4 kHz and (B) all fibers with CF < 4 kHz. Data from exposed fibers is overlaid in red. The fiber sample is the same as that shown in Figure 8.

5.2.4 Other Response Properties

While it appears that tuning is normal, the altered SR distribution suggests that just one population of fibers is missing. Here we look at other response properties and ask whether, post-exposure, low-, medium- and high-SR fibers respond similarly to their pre-exposure counterparts.

One important question is whether the relationship between threshold at CF and SR is maintained among surviving fibers. To normalize for CF-related differences, threshold for each fiber is expressed relative to the average for high-SR fibers in the same animal at a similar CF. In Figure 11 we see that control thresholds decrease with increasing SR, and we see that the relation is essentially unchanged in the exposed ear, i.e. the few remaining low-SR fibers in the exposed ears still show higher thresholds than the high-SR fibers with similar CF. An analysis of covariance, which compares linear regressions of two groups of data, shows that the distribution of relative threshold vs. SR does not change post exposure (ANOCOVA, $P > 0.05$ for both slope and y-intercept).

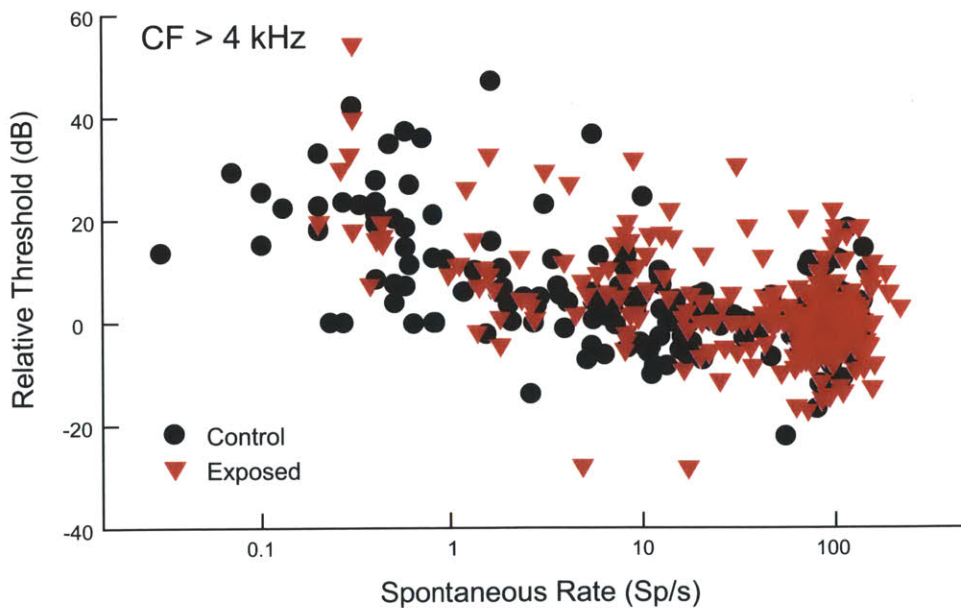


Figure 11 The relation between threshold and SR is maintained in exposed ears

The threshold for each AN fiber is expressed relative to the mean threshold for high-SR fibers with the same CF in the same animal. Only fibers with CF > 4 kHz are shown. In the few low-SR fibers remaining in exposed ears, relative thresholds are within the normal range. Linear regressions of exposed versus control data are not significantly different (ANOCOVA, $T > 0.05$ for both slope and y-intercept).

Figure 12 presents two additional metrics of AN responses. The dynamic range of a fiber is defined as the range of stimulus intensities over which the fiber changes its discharge rate. In the control ear, low-SR fibers have the widest dynamic ranges (Figure 12A), as reported by others (Taberner and Liberman, 2005). Correspondingly, in the exposed ears, the remaining low- and med-SR fibers also have the largest dynamic ranges.

The sharpness of tuning, Q_{10dB} (Figure 12B), is defined as the bandwidth 10 dB over CF threshold normalized to the CF [$Q = CF/BW$]. There was no systematic change in sharpness of tuning between control and exposed ears. This is not unexpected, as sharpness of tuning arises predominately from the active properties of the outer hair cells, which appear relatively unaffected, as assessed by DPOAE responses (Figure 5).

Post stimulus time histograms (PSTHs) were recorded at CF, 30 dB above threshold. These were used to evaluate several additional aspects of synaptic function. The PSTHs reveal a prominent post-adaptation in the discharge rate. In response to a 50-msec tone burst, as in the present study, discharge rate is maximum near stimulus onset and decays towards a steady-state value. The decay in discharge rate is typically best fit as the sum of two exponentials: one with a more rapid time constant (< 10 ms, Figure 13A) and one with a longer time constant (~ 20 -40 ms, Figure 13B). This adaptation process is thought to reflect the depletion of readily releasable pool of synaptic vesicles during the response to a tone (Westerman and Smith, 1984; Glowatzki et al., 2008; Buran et al., 2010). Noise-induced synaptic changes might be seen in altered time constants of post-onset adaptation, however, the values extracted from PSTHs in the exposed ear appear unchanged from the control.

The PSTHs can also be used to evaluate the timing and precision of AN firing. First-spike latency (Figure 13C) reflects how rapidly a neuron responds at the onset of a stimulus. This response is dependent upon the transmission time through the middle ear, the propagation time through the cochlea, and the synaptic delay at the IHC/AN synapse. First-spike latencies were not significantly affected by the noise exposure. The variance of the first-spike latency (Figure 13D) reflects the reliability of firing. This was severely disrupted in mutant mice missing most of their synaptic ribbons (Buran et al., 2010), and the lack of observable changes post exposure provide additional evidence that remaining fibers are functioning normally.

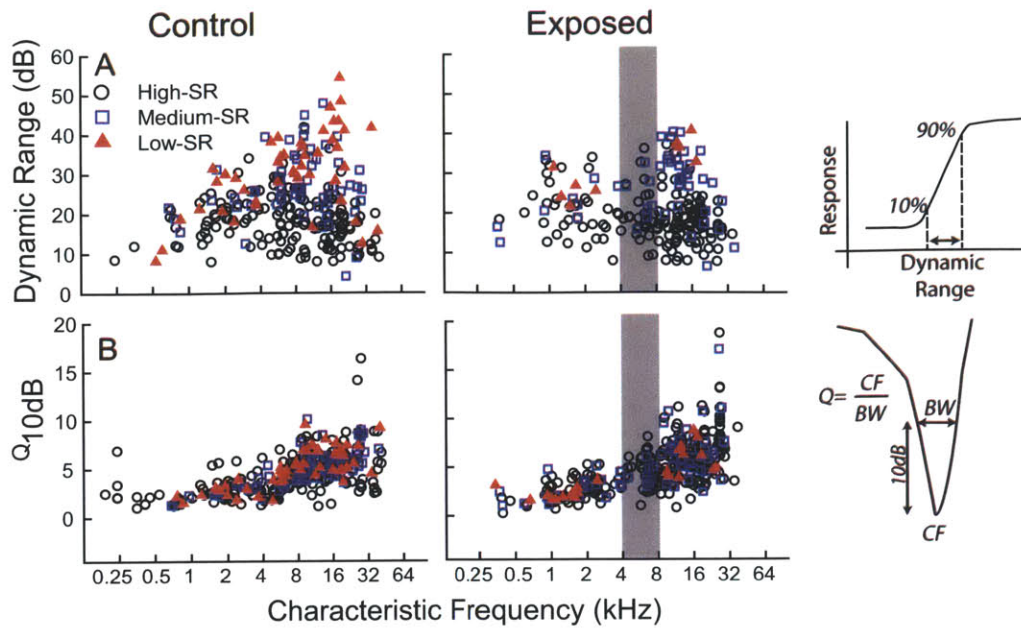


Figure 12 Tuning and dynamic range of AN fibers remain unchanged in the exposed ears

(A) To extract dynamic range, the rate-level function was fit with a model (see Methods) and the difference, in dB, between the levels eliciting 90% and 10% of the maximum driven rate (maximum rate minus spontaneous rate) was computed. (B) Sharpness of tuning is extracted from the tuning curve and is defined as the ratio between the bandwidth at 10 dB above CF threshold to the threshold. Not all metrics were recorded from all neurons due to limitations in recording time. Symbol key in A applies to all panels.

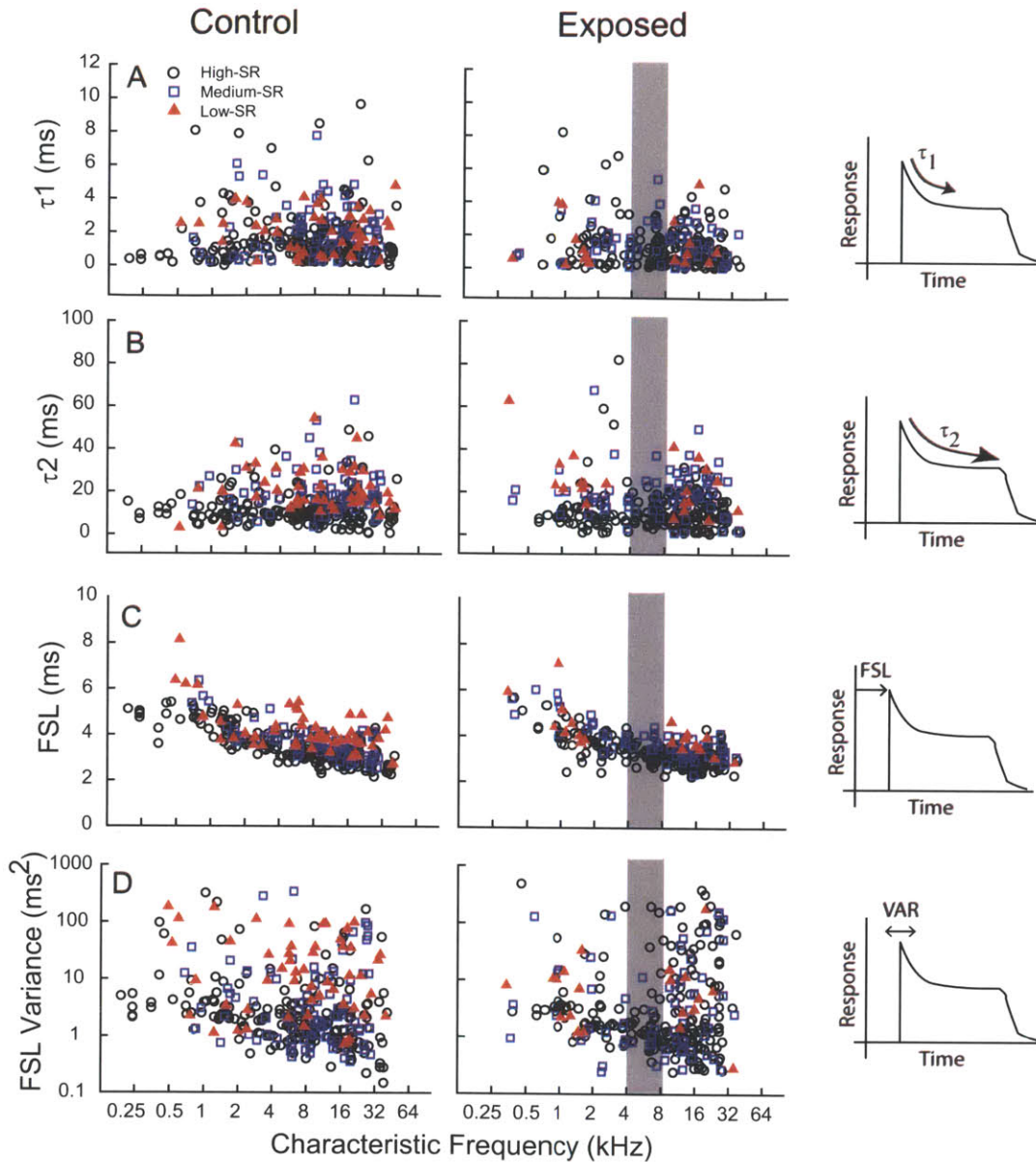


Figure 13 Basic properties of the PSTHs in response to CF tone bursts remain unchanged in the exposed ears

All data here are extracted from 200 presentations of CF tone bursts at 30 dB above threshold. The first (A) and second (B) time constants (τ_1 and τ_2) of post-onset adaptation are defined by the double exponential decay function that provides the best fit to the first 85 ms of the PSTH. Data were excluded if the double-exponential fit returned values of $\tau < 0$ or $\tau > 100$ ms. (C) First-spike latency (FSL) is defined as mode of a histogram generated from the first spike in response to each tone burst, calculated with a bin width of 0.1 ms. (D) First spike latency variance reflects the timing precision of the first spike, calculated as the square of the standard deviation of the FSL. Symbol key in A applies to all panels.

5.3 Forward Masking

Forward masking at the neural level describes the phenomenon whereby the presence of a one stimulus (masker) increases the detection threshold for a subsequent stimulus (probe) presented within a few hundred msec after the termination of the masker. The phenomenon is thought to arise because the masker depletes the pool of readily releasable vesicles at the IHC/AN synapse, and the recovery behavior of the probe response reflects the restocking of that pool ((Harris and Dallos, 1979)).

During presentation of the masking tone, AN responses decline from their initial peak firing rate down to a steady state, (Westerman and Smith, 1984; Spassova et al., 2004). At the conclusion of the masking tone, the readily available vesicle pool begins to recover, and as such, the response to probe tones presented with increasing delay (masker-probe interval) will recover to their unmasked firing rate. At the level of single AN fibers, systematic SR-related differences in the recovery from forward masking have been reported (Relkin and Doucet, 1991). Recovery from forward masking can also be evaluated using CAP responses (Relkin and Turner, 1988; Relkin and Smith, 1991), where prior work has suggested that the selective loss of low-SR fibers in the aging gerbil can be detected via changes in the CAP forward masking functions (Relkin et al., 1995).

5.3.1 Forward Masking at the Single Fiber Level

Tone-on-tone forward masking was evaluated in a large subset of control and exposed fibers in this study. A 100 ms masking tone was presented at CF, 40 dB over threshold to drive the fiber close to its maximum firing rate without risking traumatic sound pressure levels. A masker-probe interval of 2-256 ms preceded the 15 ms probe tone also at CF, 40 dB above threshold. PSTHs were recorded for each presentation, and averaged 50 times per interval. This generated a PSTH for each masker-probe interval, a representative example of which can be seen in Figure 14A,B,C.

To derive a single metric of forward masking for each fiber, the peak response rates to the masker and the probe were extracted for each interval tested. To normalize for different maximum firing rates between fibers, the probe response was normalized to the control, giving us a normalized decrement (ND), where

$$ND = \frac{\text{Masker Peak Rate} - \text{Probe Peak Rate}}{\text{Masker Peak Rate} - \text{Masker Adapted Rate}}$$

The adapted response rate to the masker was taken as the maximum attainable suppression, so the normalized decrement is 1 when the probe response is equal to the adapted masker response (i.e. the average value of the masker PSTH, from 85 to 95 ms, shown with a bracket in Figure 14C). The masker and probe responses are plotted against probe delay in Figure 14D, and the

recovery of the probe response with increasing interval can be seen. Normalized decrement for the same fiber is plotted in Figure 14E. Fitting the data with a straight line on the semi-log axes defines the value along the x-axis where $y=0$, which we call the “recovery time” for that fiber.

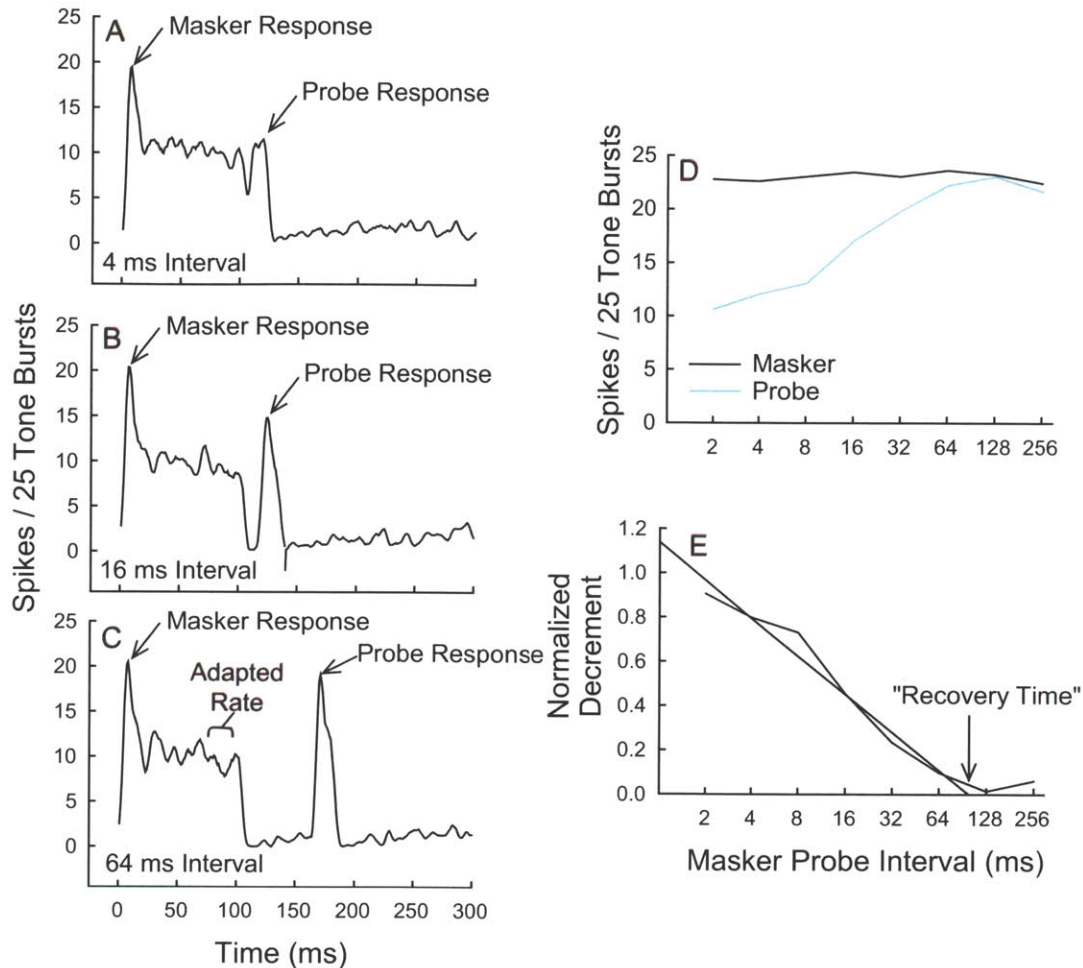


Figure 14 Forward masking analysis in single AN Fibers

Forward masking was measured in a subset of AN fibers. A 100ms masking tone was presented at CF, 40 dB above threshold, followed after a delay from 2 to 256ms, by a 15ms probe tone at the same frequency and level. (A) Example PSTHs at 4, 16, and 64ms masker-probe intervals. Peak responses from masker and probe are marked with arrows. Data represent 25-50 presentations of the stimulus. (B) Peak responses from the masker and probe are plotted against the masker-probe interval. Probe response recovers with increasing masker-probe interval. (E) Normalized decrement is calculated from the data in (D), normalizing the probe response to the peak response rate, and adjusting for the adapted rate. $\text{Normalized Decrement} = (\text{Masker Peak Rate} - \text{Probe Peak Rate}) / (\text{Masker Peak Rate} - \text{Masker Adapted Rate})$. The first 64ms of data are fit with a straight line on a log axis. The x-axis intercept provides the “recovery time” for that AN fiber.

The recovery time was calculated for 47 control fibers, and 45 exposed fibers. In Figure 15 we see the recovery times plotted against SR. In unexposed ears, low-SR fibers have the longest recovery times (all longer than 100 ms), med-SR fibers have intermediate recovery times, and the high-SR fibers have the fastest recovery times (all shorter than approximately 100 ms). In the few low-SR fibers from exposed ears, recovery times are close to the normal range. An analysis of covariance, which compares linear regressions of two groups of data, shows that the dependence of recovery time on SR does not change post exposure (ANOCOVA, $P > 0.05$ for both slope and y-intercept). A Mann-Whitney rank sum test applied to low- and med-SR data only (shaded area, Figure 15) also indicates that differences between groups are not statistically significant ($P \gg 0.05$).

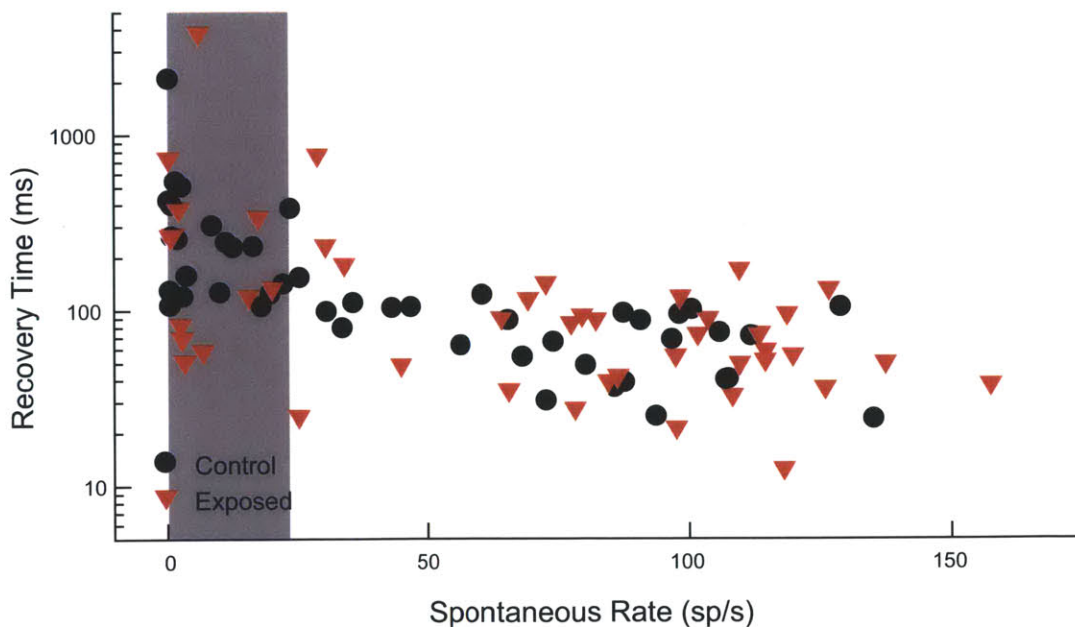


Figure 15 Forward masking recovery time is unchanged in exposed ears

The recovery time from forward masking is plotted against SR. Low- and med-SR fibers (grey shaded area) have longer recovery times (>100 ms), and high SR fibers have shorter recovery times (<100 ms). AN fibers in exposed ears have responses that appear similar to unexposed controls. Linear regressions of exposed versus control data are not significantly different (ANOCOVA, $T > 0.05$ for both slope and y-intercept). For low- and med-SR fibers separately (SR < 20 , shaded area) there was not a statistically significant difference between control and exposed fibers (Mann-Whitney rank sum test, $P \gg 0.05$).

5.3.2 Forward Masking in the CAP

The differences in recovery times across SR suggest that there may be a difference in the CAP forward-masking function because a large proportion of low-SR fibers are missing. Missing low-SR fibers as found in section 5.2.3 should reduce the slowly recovering nerve population, leaving the CAP response dominated by the rapidly recovering high-SR fibers.

The forward masked CAP response was recorded by measuring the response to 5 ms tone pips presented at 17.54 kHz, preceded by a 100 ms masker tone at 17.54 kHz. 17.54 kHz was chosen because it is in middle of the region where the maximum synaptic disruption was seen (See Section 5.4). Both tones were presented 40 dB over the CAP threshold at 17.54 kHz, a level sufficiently intense to excite both low- and high-SR fibers. Masker-probe interval was varied, from 8 ms – 1024 ms, and waveforms were averaged 32 times. Normalized decrement was defined similarly to the single fiber data, where:

$$\text{Normalized Decrement} = \frac{\text{Control Response} - \text{Probe Response}}{\text{Control Response}}$$

The addition of the “adapted rate” term in the single fiber analysis scales the single fiber normalized decrement to range from 1- not masked to 0- fully masked. Similarly, normalized decrement for the CAP response goes from 1- not masked to 0- fully masked. This difference is that the adapted rate represents the maximum measurable masking at the single fiber level, and a CAP of 0 μV represents maximum masking (i.e. no response). Figure 17 shows the average ND against masker-probe interval for control and exposed animals. The difference between groups was not statistically significant (ANOVA, $P \gg 0.05$).

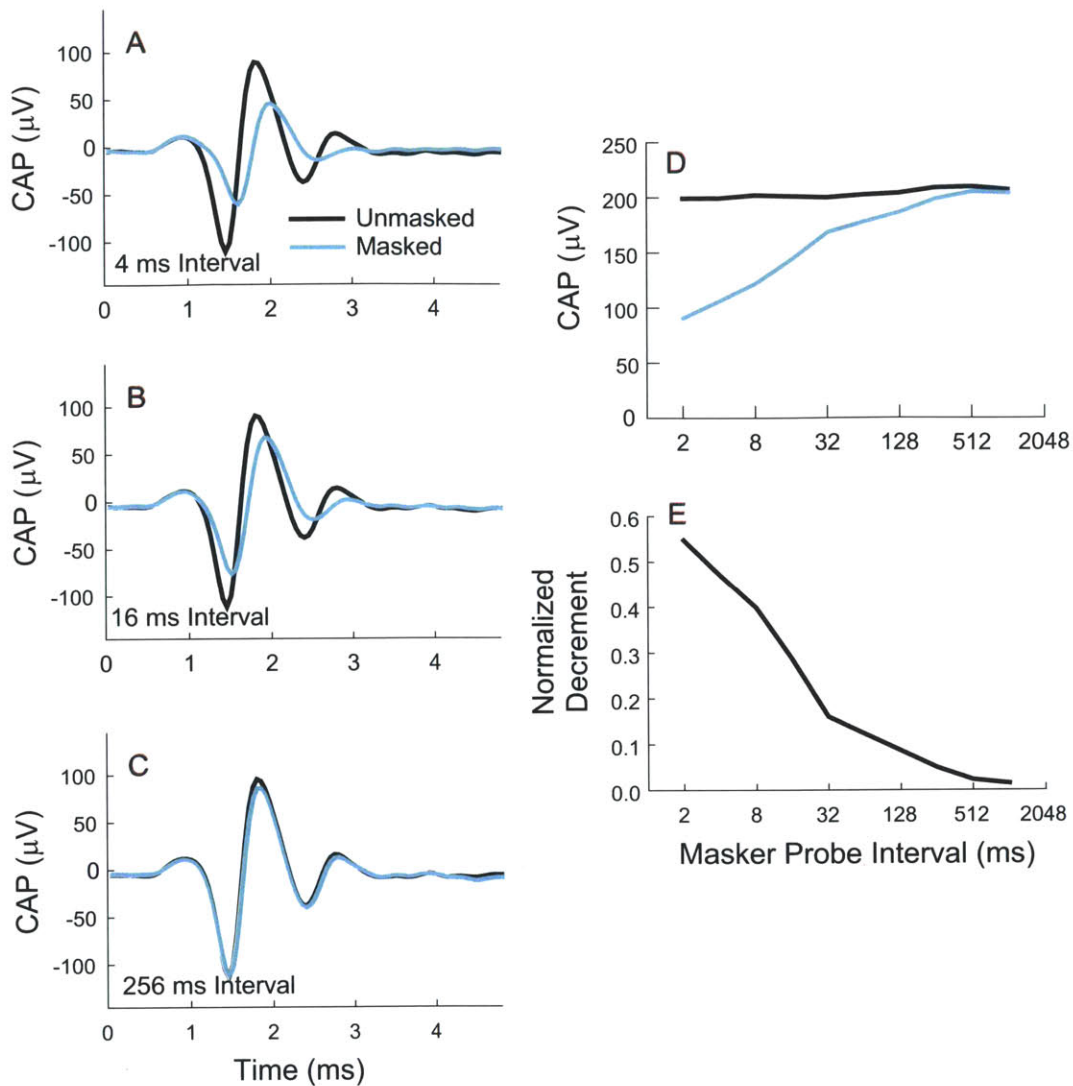


Figure 16 CAP Forward Masking Analysis

CAP responses were recorded in a forward-masking paradigm. A probe tone was presented at varying delays following the presentation of a 100 ms masking tone. Both the masker and probe tone were at the same frequency and intensity, and control probe responses with no masker were interleaved between trials. (D) The peak-to-peak amplitude of masked and unmasked probe responses is plotted vs masker-probe interval. (E) Normalized Decrement is extracted from the data in D: $\text{Normalized Decrement} = (\text{Unmasked} - \text{Masked}) / \text{Unmasked}$.

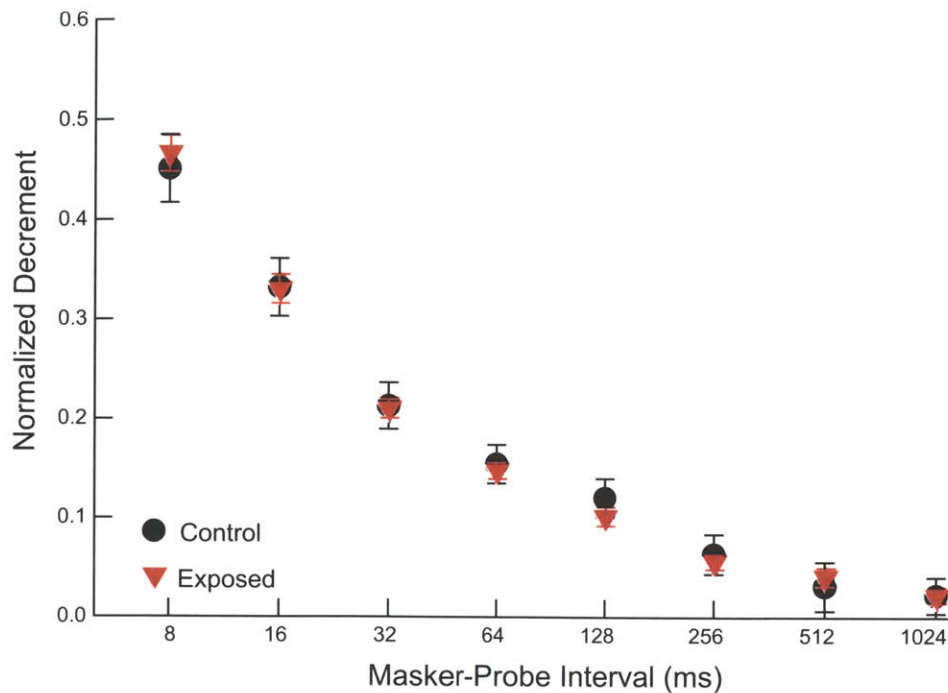


Figure 17 CAP Forward Masking functions are unchanged in the exposed ears

Mean Forward Masking functions, as derived, as shown in Figure 16, from the CAP in unexposed control ears ($n = 11$) and exposed ears ($n = 13$). Stimuli were 40 dB above CAP threshold at 17.54 kHz. Differences between the means were not statistically significant (ANOVA, $P \gg 0.05$)

5.3.3 Low- and High-SR Contributions to the CAP

Relkin and colleagues suggest that the CAP forward masking functions such as those in Figure 16 are well fit by two straight lines – a steep recovery at short masker-probe intervals dominated by contributions from high-SR fibers and a shallower segment at longer masker probe intervals that reflects the contributions of the slowly recovering low-SR fibers (Relkin and Doucet, 1991). Our data did have a two-segment normalized decrement function, and we applied an analysis modeled after Relkin et al. which we used to evaluate the relative contributions of low- and high-SR fibers (Relkin and Doucet, 1991). The CAP normalized decrement functions were fit by the sum of two straight lines on a logarithmic interval scale. The fast component was a line fit through intervals ≤ 64 ms, and the slow component for intervals ≥ 128 ms. This shows us the fast component recovering in ~ 65 ms for both control and exposed ears, and is consistent with the single fiber data (Figure 15) showing high-SR recovery in 20-100 ms. Similarly, in the control ear, the slow component recovered in 1280 ms, which is reasonable given that low-SR fibers recovery times range from 100 to 3000 ms. When we consider the relative contributions

of low- and high-SR components in this analysis, the exposed ear does have a trend in the correct direction, where there is a reduced contribution from slow component. Despite no statistically significant difference in the means, the data in Figure 18 shows that the slow component is depressed, and that the fast component contributes more. Quantitatively, we calculate the area under the curve for the low-SR fibers, from 8-1024 ms, and see a 19% reduction in area post exposure, consistent with the suggestion that roughly 20% of the low- and med-SR fibers are missing.

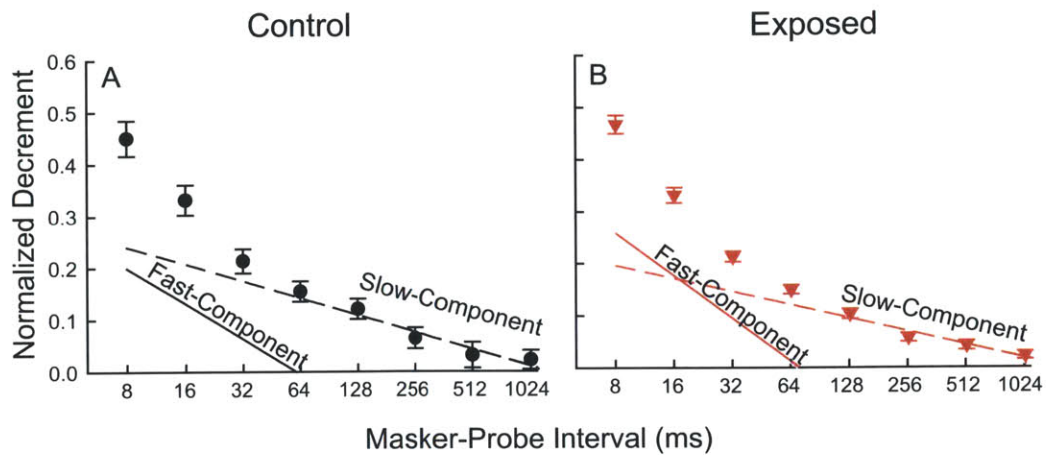


Figure 18 Modeling the Low- and High-SR contributions to CAP forward masking functions

For control ears (A) and exposed ears (B). Data was fit by a two segment straight line on a log time axis. This two segment line can be modeled as the sum of two straight lines, a fast component of which represents the putative contribution from high-SR fibers, and the other that represents the contribution from low-SR fibers.

5.4 Histology of Ribbon Loss

5.4.1 Confocal Imaging

Control and exposed cochleae were dissected and immunostained for a variety of cellular markers including CtBP2, a major component of pre-synaptic ribbons, Myosin VIIa to stain the IHC cytoplasm, and GluR2 to stain for post-synaptic glutamate receptor patches. Figure 19 shows a representative example from both a control and exposed cochlea, at the 32 kHz region, including both the view from the epithelial surface (xy projection) and the cross-sectional view (yz projection).

In the control ear, this immunostaining shows afferent synapses arrayed around the IHC basolateral membrane in the subnuclear zone. Each synapse is clearly identified by a CtBP2-positive (red channel) synaptic ribbon within the IHC and a closely apposed GluR2-positive

(green channel) post-synaptic receptor patch. This immunostaining patterns is consistent with the view arising from serial-section ultrastructural studies (Liberman, 1980; Merchan-Perez and Liberman, 1996), where it has been shown that the afferent fibers contacting the IHC are almost all unbranched, each contacting a single IHC via single terminal bouton, which forms a single synaptic plaque of closely apposed pre- and post-synaptic membrane specialization, at which a single pre-synaptic ribbon is located on the IHC side.

In the noise-exposed tissue the synaptic organization appears disrupted. Most importantly, there appear to be fewer synapses. In addition, the synapses are not as neatly organized along the basolateral surface of the IHCs. Lastly, one can see orphan ribbons, without an associated GluR2 patch (white arrow in Figure 19C) and orphan GluR2 patches without an associated ribbon (arrowhead in Figure 19A). These orphans were seen in control and exposed tissue, and differences will be quantified later in Section 5.4.352.

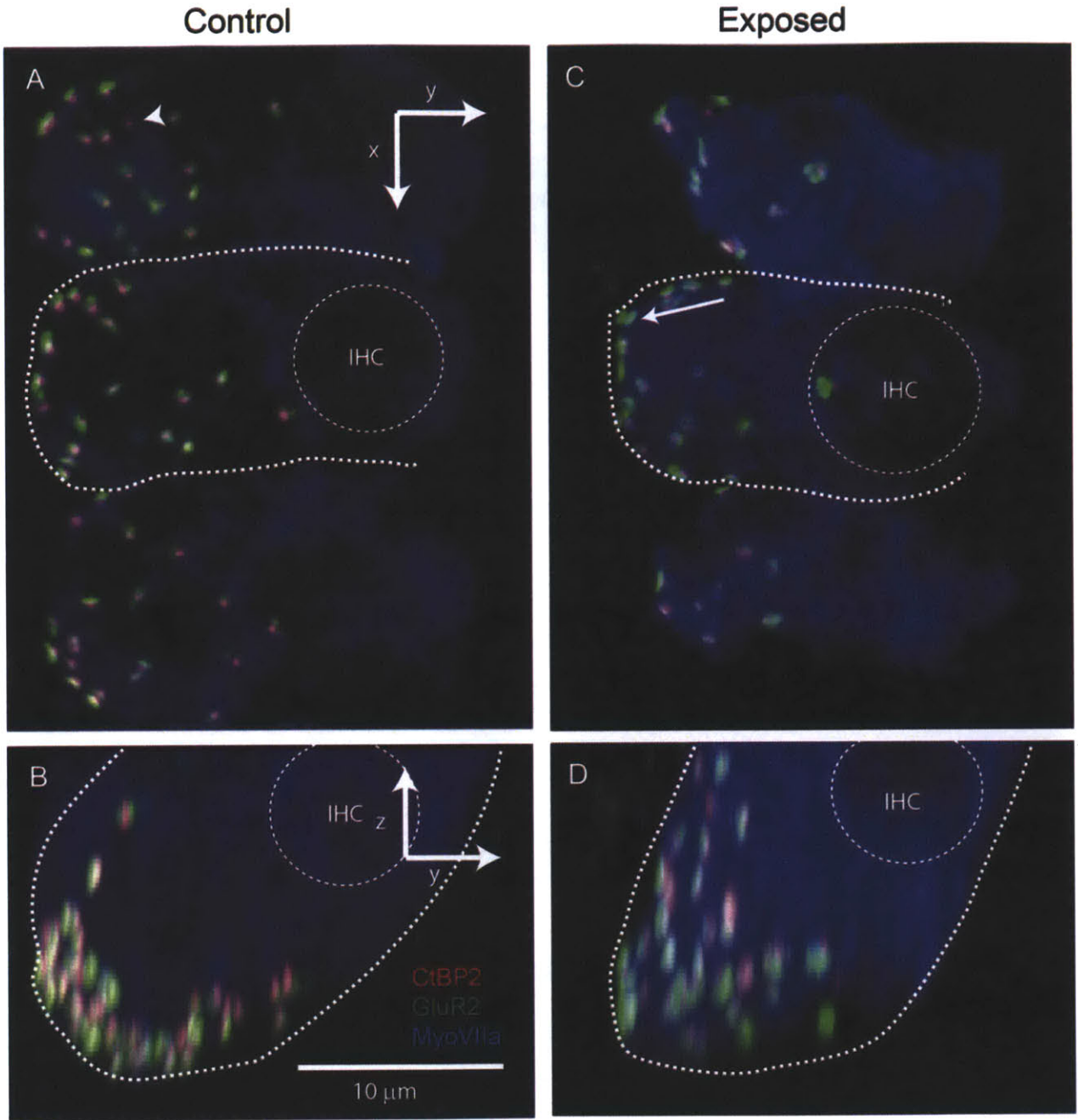


Figure 19 Confocal analysis of noise-induced synaptic degeneration.

Cochlear tissue was triple-stained for CtBP2 (red), GluR2 (green), and Myosin VIIa (blue). Example images from the 32kHz region of a control ear (A,B) and exposed ear (C,D) shows the maximum projection of an xy surface-view of 3 adjacent IHC (A,C) and a yz side-view maximum projection of the same 3 IHCs respectively (B,D). For all images the outer hair cell region would be towards positive y values out of the field of view. The IHC border and nucleus is outlined with a dashed line. The white arrow in C points to a GluR2 patch without a ribbon, and the arrowhead in A points to a ribbon without a GluR2 patch. Scale bar in B applies to all panels.

We used Amira software to count synaptic elements in each confocal z-stack. The analysis is done in 3-D, thereby eliminating any undercounting issues arising from superposition of elements in the maximum projections (See Methods). The output of the Amira analysis included the xyz coordinates of each synaptic element (ribbon or receptor patch) as well as its volume. For each z-stack, the number of IHCs contained was also counted so that data could be expressed on a per IHC basis.

In the normal ear, the number of synapses per IHC varies with cochlear location, however, it peaks at roughly 19/IHC, in the middle of the cochlear spiral, as shown in Figure 18A. This value is consistent with numbers obtained in serial section ultrastructural studies in the guinea pig (Hashimoto et al., 1990). In the exposed ear, the mean number of synaptic ribbons is reduced compared to control ears (Figure 20B) for all cochlear frequencies at and above the exposure band. Differences between the means were statistically significant at 32 and 45 kHz (ANOVA, $P < 0.01$). Normalizing the counts in exposed ears to the values obtained in unexposed controls (Figure 20B) shows that there is approximately a 10% reduction in ribbons at 16kHz following noise exposure, which falls off to a 25% reduction by 45 kHz.

The skewing of synaptic degeneration toward regions above the exposure band is consistent with the cochlear pattern observed in prior studies in both mouse (Kujawa and Liberman, 2009) and guinea pig (Lin et al., 2011). It is also consistent with the more general observation that noise-induced damage to both hair cells and cochlear thresholds tends to be maximal at frequencies above the exposure band – a phenomenon well documented and explained by current understanding of the non-linearities in cochlear mechanics (Robles and Ruggero, 2001).

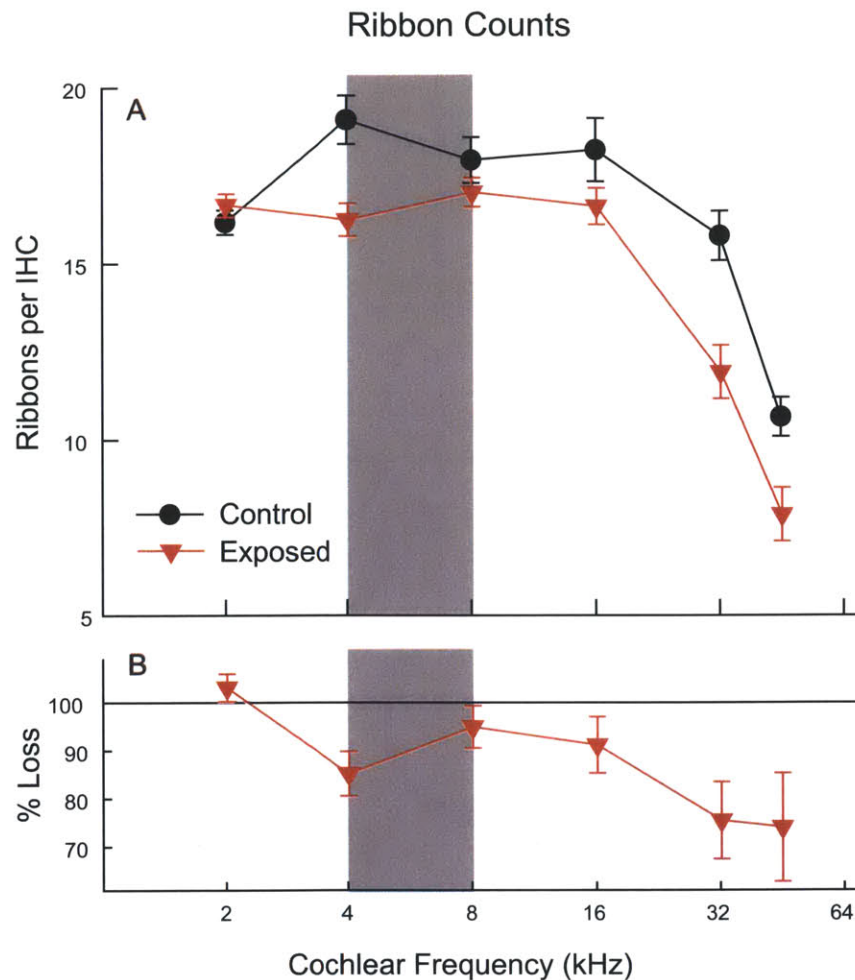


Figure 20 Synaptic ribbon counts are reduced in noise-damaged cochlear regions.

(A) Mean numbers of ribbons per IHC are plotted against cochlear frequency. Error bars indicate standard error of the mean. (B) Same data as in A, replotted to express the counts in exposed ears as % loss. Data in both panels are from 5 control, and 14 exposed ears. In each cochlear region, in each ear, two adjacent z-stacks were acquired, each including 75 μm of cochlear length (encompassing 7-9 adjacent IHCs). Ribbon counts were made using the connected components feature in Amira imaging software (see Methods).

5.4.2 Spatial Distribution of Ribbons

In a normal IHC, there is a gradient of SR from low to high as you move from the modiolar to pillar side of the hair cell (Merchan-Perez and Liberman, 1996): see Figure 1. Correspondingly, ribbon volumes and GluR2 patch size also change with synaptic location around the IHC circumference (Liberman et al., 2011). In order to evaluate the modiolar-pillar distribution of sizes of pre-synaptic ribbons and post-synaptic receptor patches, we manipulated the z-stacks to

transform the x,y,z axes, as acquired, into a set of axes more amenable to the analysis of these modiolar-pillar gradients. As demonstrated in Figure 21, we 1) rotated each stack in the yz plane to make the long axis of the IHC parallel to the z axis, 2) moved the y=0 point to the middle of the IHC such that modiolar positions were at negative y values and pillar positions were at positive y values, and 3) set the z=0 point to the location of the synaptic element farthest from the IHC hair bundles.

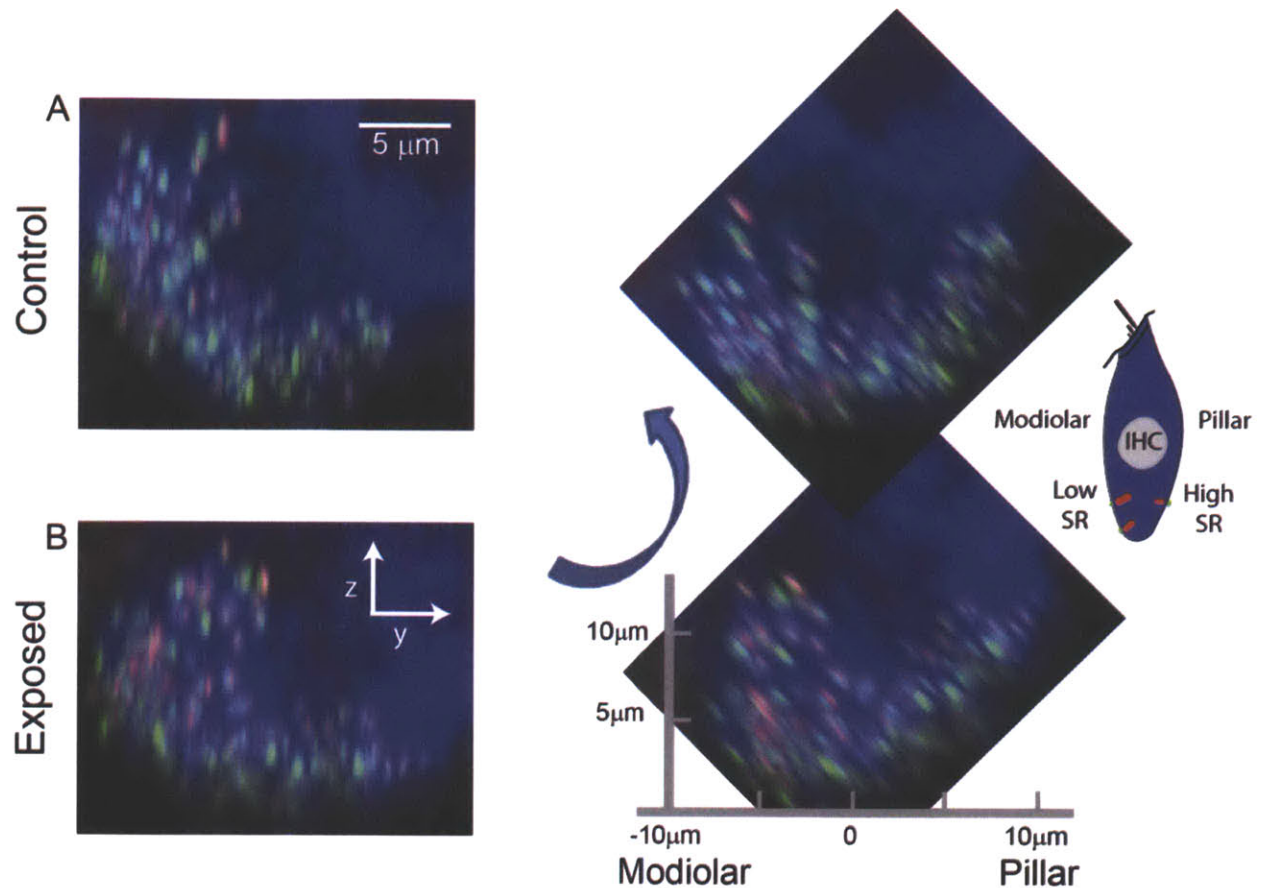


Figure 21 Illustration of the spatial transformations applied to assess the spatial organization of synaptic puncta on the pillar vs. modiolar sides of the IHC.

Maximum yz projections from a representative confocal z-stack from the 16 kHz region of a control (A) and an exposed (B) ear. To establish a uniform coordinate system to assess the locations of synaptic components, each z-stack was rotated 45 degrees counterclockwise, in the yz plane, to “correct” for the tilt of the IHCs in these whole mounts. The new y axis was zeroed to a position corresponding the median y value for all the synapses in the stack, and the new z axis was zeroed to the location of the “deepest” synaptic element, i.e. the value farthest from the IHC stereocilia.

Results of this coordinate transformation are seen in Figure 22 with data superimposed from control (A,B,C) and exposed (D,E,F) ears, at 2, 16 and 32 kHz. To better represent the morphological gradients, we also made symbol size proportional to the cross-sectional area of each synaptic element.

In the control ear, at all cochlear frequency regions evaluated, there is a tendency for large ribbons on the modiolar side and smaller ribbons on the pillar side, as described in prior electron microscopic study in cat (Merchan-Perez and Liberman, 1996) and prior confocal analysis in mouse (Liberman et al., 2011). Comparison of panels A, B and C to panels D, E, and F suggests that, in the exposed ear, this clear modiolar-pillar gradient in ribbon size is disrupted, especially at the highest frequency region (32 kHz). We binned the ribbon size data according to modiolar-pillar location, as shown panels G, H and I of Figure 22. These mean data show more quantitatively, that the noise-induced changes are most striking at the 32 kHz region, and that there is a significant increase in ribbon size on the pillar sides of IHC in this region after noise exposure. Either synapses with large ribbons have moved from the modiolar to the pillar side, or ribbons on the pillar side have hypertrophied. Ignoring points at the extreme modiolar and pillar locations ($-10\ \mu\text{m}$ and $+10\ \mu\text{m}$), where relatively few synapses were found, there was no statistical difference in ribbon volume versus location at 2 kHz. At 16 kHz and 32 kHz, ribbons were significantly larger in the bins centered at $+2\ \mu\text{m}$ and $+6\ \mu\text{m}$ relative to the center of the IHC (ANOVA, $P < 0.05$). The increased scatter in the depth of ribbons post exposure likely reflects reorganization of the IHC synapse as more ribbons appear further from the hair cell base.

The same analysis of volume and location was carried out for the GluR2 staining in the same ears (Figure 23). In the mean data from control ears (panels G, H and I), a modiolar-pillar gradient in receptor patch size is not obvious. The most striking effect of the noise exposure is a decrease in receptor patch volume across both pillar and modiolar faces and at all cochlear frequency regions evaluated. At 2 kHz, this decrease was significant for all modiolar-pillar bins except the bin centered at $+6\ \mu\text{m}$ (ANOVA, $P < 0.05$). At 16 kHz the decrease was significant in all but the bin centered at $+10\ \mu\text{m}$ (ANOVA, $P \ll 0.01$), and at 32 kHz the decreases were significant in the bins centered at -2 , 2 , and $6\ \mu\text{m}$ (ANOVA, $P < 0.01$).

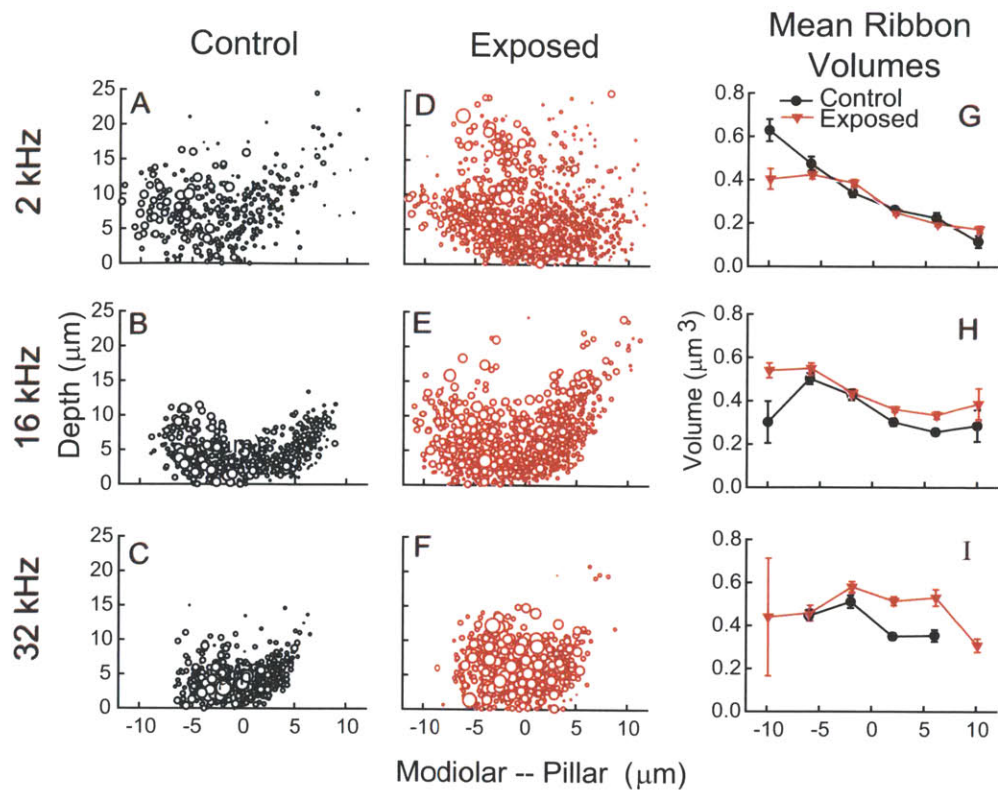


Figure 22 Ribbon volume is increased, and the normal modiolar-pillar gradient is disrupted, in noise-damaged cochlear regions.

Ribbon location is plotted for three frequency regions (2, 16, 32 kHz). At each region, data from 2 control and 6 exposed ears are superimposed. Symbol size in the scatter plots (A-F) is proportional to the cross sectional area for each ribbon, derived by considering the measured volume as that of a perfect sphere. Data in panels G-I show the same data set shown in Panels A-F, separated for averaging into adjacent 4 μm bins of modiolar-pillar position. Error bars show $\pm\text{SEM}$. The derivation of the modiolar-pillar position and the depth of each ribbon is described in Figure 21.

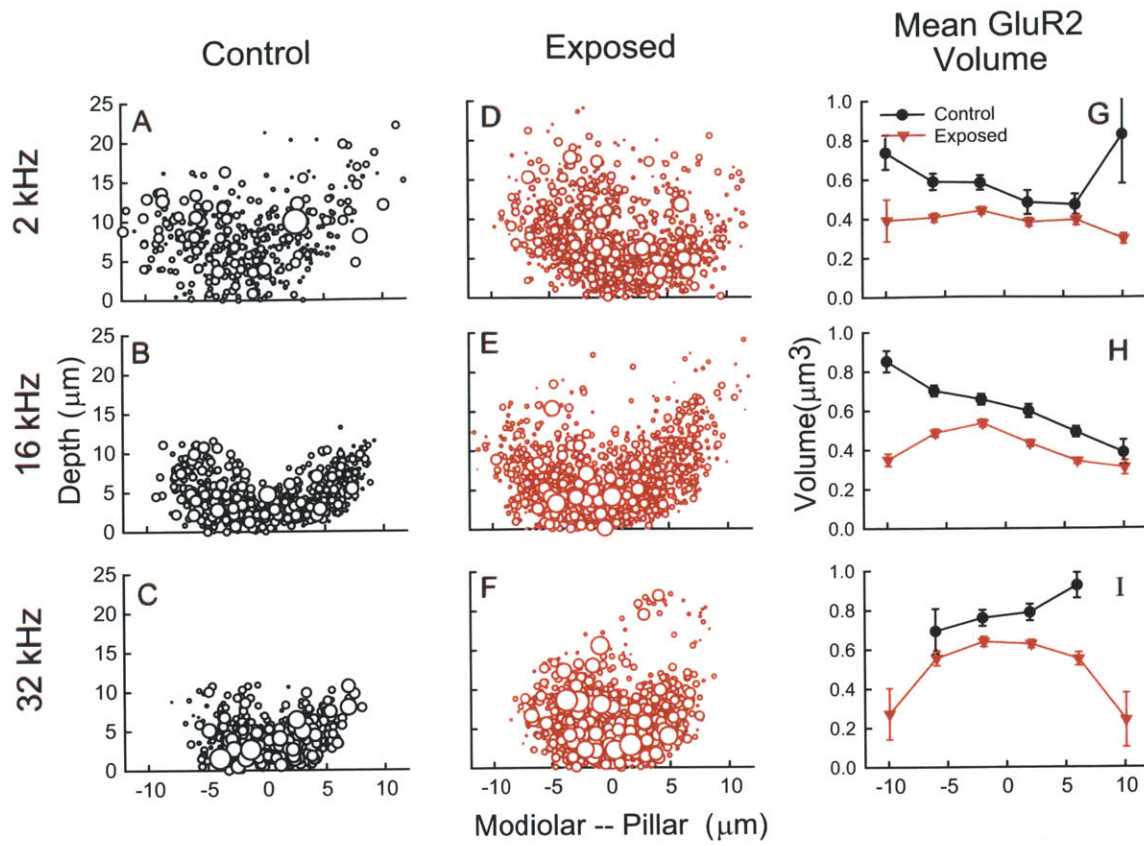


Figure 23 The volume of glutamate receptor patches is reduced throughout much of the noise-exposed cochlea.

The spatial distribution and size of glutamate receptor patches is plotted for three frequency regions (2, 16, 32 kHz) – in each panel (A-F) data for 2 control and 6 exposed ears are superimposed. Other conventions for data display are as described for Figure 22.

5.4.3 Synaptic Ribbons and Post-Synaptic Markers

Qualitative analysis of the confocal projections suggested that, after noise exposure, it was more common to see orphan ribbons without post-synaptic receptor patches and post-synaptic receptor patches without closely juxtaposed pre-synaptic ribbons (See orphans in Figure 19C). To assess the numbers of orphan elements more quantitatively requires disambiguating the superposition of elements that arises when the 3-D z-stack is viewed as a 2-D projection. To do this, we used custom software to take the xyz coordinates of all the synaptic elements (either ribbons or receptor patches) identified using the Amira software (See Methods) and then redisplay the synaptic elements in each z-stack as a thumbnail array of mini-projections, each including only the voxel space within 1.5 μm of each previously identified synaptic element.

Figure 24B shows 12 of these thumbnails from one z-stack: each in the top cluster is centered on the xyz location of a GluR2 patch, each in the bottom cluster is centered on the xyz location of a ribbon. With such thumbnail projections, it becomes easy to clearly identify and count the unpaired entries (black arrows in Figure 24B).

As shown in Figure 25A, in control ears, less than 3% of ribbons lack a closely apposed glutamate receptor patch, and less than 5% of the identified GluR2 patches lack a closely apposed pre-synaptic ribbon. In the exposed ear, there is a small but statistically significant increase in the numbers of orphan ribbons at 16 kHz (4%, ANOVA Pairwise Comparison, $P < 0.05$). In Figure 25B there was also a significant increase in the number of orphaned receptors at 16 and 32 kHz (ANOVA Pairwise Comparison, $P < 0.05$).

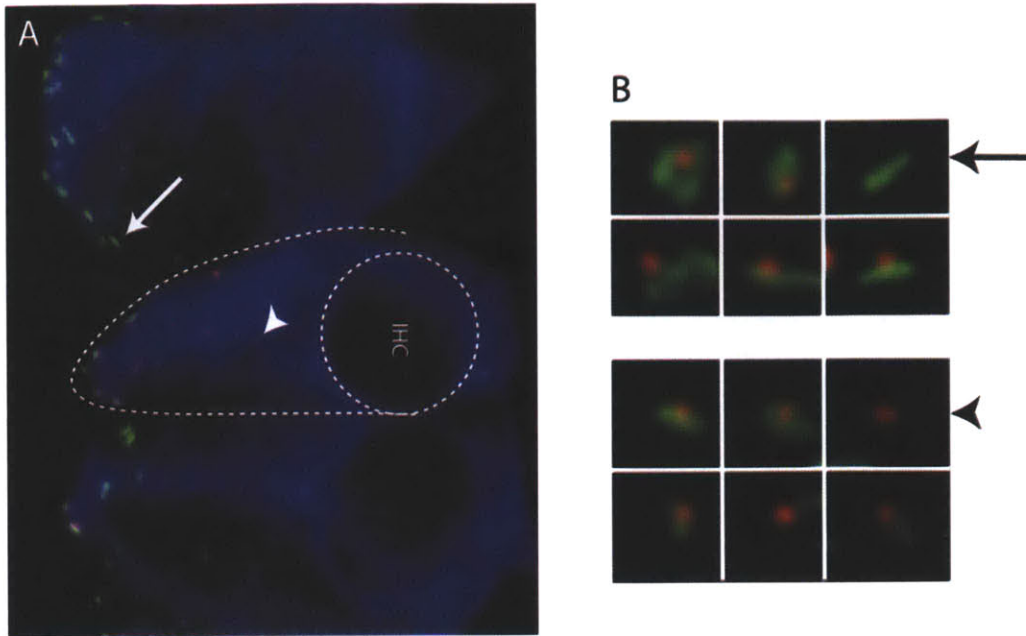


Figure 24 Analysis of the pairing of pre-synaptic ribbons with post-synaptic receptors

(A) An xy projection of 3 IHCs triple stained for CtBP2 (red), GluR2 (green), and Myosin VIIa (blue) from control tissue at 32 kHz. The white arrow points at a GluR2 patch with no opposed ribbon, and the arrowhead points to a ribbon with no opposed GluR2 patch. One IHC and the IHC nucleus is outlined in a dashed line. (B) To quantify the juxtaposition of pre and post-synaptic elements, each image stack was re-displayed using custom software to produce a high-power projection of the voxel space immediately around (i.e. within 1.5 μm of) each pre- or post-synaptic element identified in the Amira analysis of connected components - see Methods). (B) These miniature re-projections were displayed as a thumbnail array, which allowed for easy identification of unpaired or GluR2 receptor patches (top, arrow) or ribbons (bottom, arrowhead).

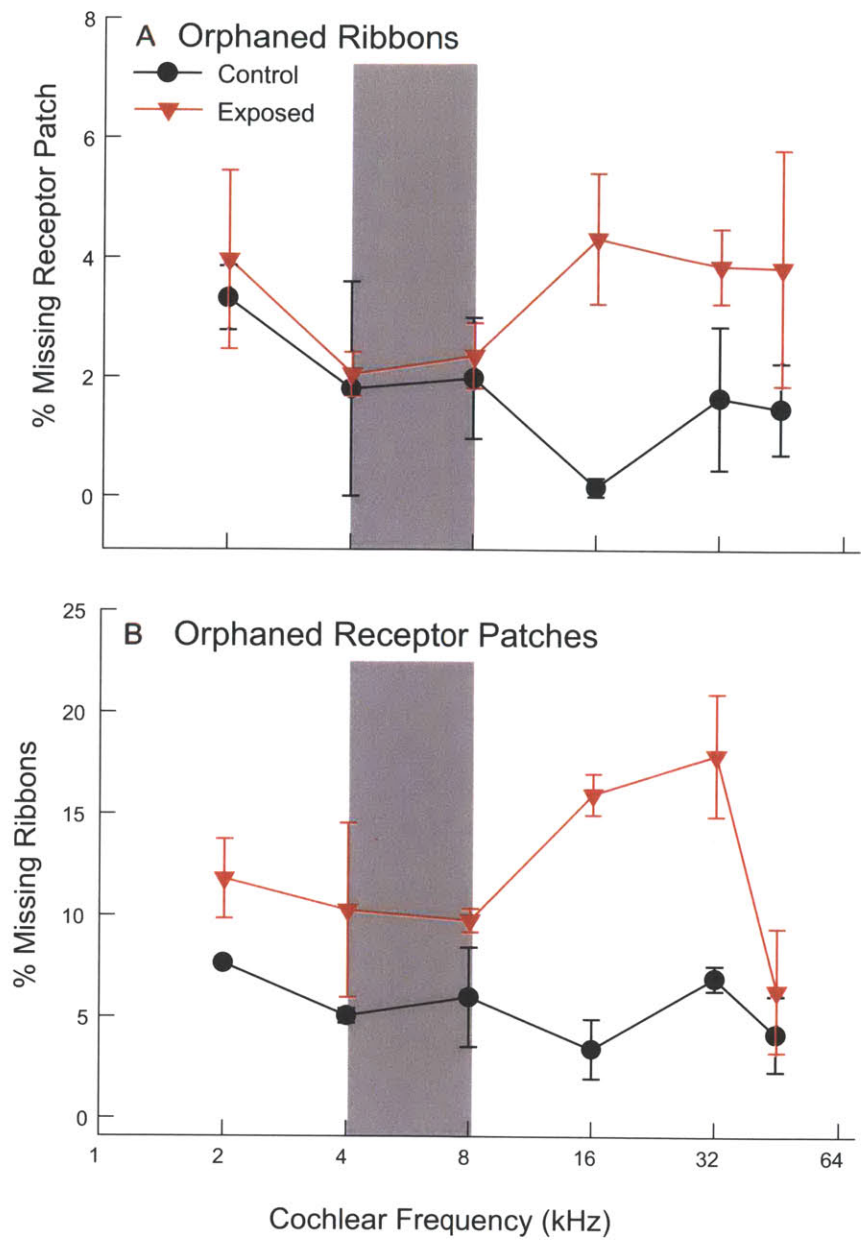


Figure 25 The frequency of orphan ribbons or glutamate receptors was increased in the noise-damaged cochlear regions.

(A) The percentage of ribbons lacking an opposed GluR2 patch. (B) The percentage of GluR2 patches lacking an associated ribbon. Data are means (\pm SEM) for data from 2 control ears and 6 exposed ears.

6 Discussion

6.1 Preservation of Threshold

The effects of noise exposure on the ear vary with exposure dosage, a combination of exposure duration and exposure intensity (OSHA, 2012). The noise exposure in this study, and studies like it (Kujawa and Liberman, 2006; Lin et al., 2011) was chosen to be as intense as possible without causing permanent threshold shifts. This presents the interesting opportunity to look at the effects of acoustic overexposure without the confound of threshold shift or any of the more severe damage that accompanies it. While we had hypothesized that threshold was maintained because the high-SR, low-TH fibers were unaffected, cochlear thresholds can in fact be very tolerant to diffuse loss of auditory neurons. Schuknecht showed that behavioral thresholds were unaffected by substantial auditory nerve losses in humans (Schuknecht, 1953). In carboplatin treated mouse ears, over 50% of IHCs were destroyed, and animals still had normal CAP thresholds (Liberman et al., 1997). The insensitivity of cochlear thresholds to diffuse neuron loss is not surprising when one considers that small increases in stimulus intensity recruit large numbers of additional fibers. More quantitatively, the sharpness of tuning Q , in Figure 12B shows us that at 16 kHz a 10 dB increase in stimulus intensity spreads excitation across an additional 3 kHz of the cochlea. With a stimulus increase of only 5 dB, the resolution of most ABR threshold paradigms, this would affect over a 1 kHz span of the cochlea at 16 kHz, on the order of an additional 30 IHCs (Taberner and Liberman, 2005). Even with only 10 fibers remaining per IHC, this would activate up to 300 additional neurons. With a unitary contribution of approximately 100 nV per fiber (Prijs, 1986) to CAP responses, a 5 dB increase in stimulus would therefore add at least 30 μ V to the summed CAP response. At a CAP criterion threshold of 15 μ V (see Figure 9), an increase of a few dB would compensate for a diffuse loss of half of the nerve fibers, at least for measures of threshold. That is, there could be a few dB of threshold shift from diffuse loss of neurons that would be essentially undetectable by standard ABR or CAP measures. However, we now know that there was selective loss of low- and med-SR fibers, which suggests that the preservation of high-SR fibers accounts for the preservation of threshold in our sound exposed guinea pigs. This does not rule out the possibility that there was some loss of high-SR fibers, but losses were clearly greater in the low-SR fiber population.

6.2 ABR wave-1 Amplitude and Loss of Synapses

Aside from preservation of threshold, the most readily accessible “phenotype” of this noise exposure is the reduction in ABR wave-1 amplitudes. The 47% reduction of wave-1 amplitude is on par with the \sim 50% decrease seen in prior studies in mouse and guinea pig (Kujawa and Liberman, 2009; Lin et al., 2011, respectively). At intensities near threshold, both control and

noise exposed ears have similar numbers of high-SR, low-threshold fibers responding, and thresholds are the same. At high stimulus intensities, the same numbers of high-SR fibers are responding, but there are fewer low-SR fibers and thus a smaller ABR response.

This reduction in ABR wave-1 amplitude at 16 kHz (47%) seems to exceed what we might expect since the synaptic count is only reduced by ~10% at the same frequency. Some, but not all, of this difference can be accounted for by the spread of excitation at high stimulus levels. At 16 kHz, the high intensity ABR reflects the response from a large portion of the basal cochlea, where the overall synaptic loss averages at least 20% (Figure 20). A 20% loss fits with the suggestion from the SR distributions that nearly 40% of low- and med-SR fibers are missing, or roughly 20% of the total fiber population (Figure 10), as the low- and med-SR fibers comprise approximately 40% of the AN in control animals (Liberman, 1978).

Synaptic ribbon counts further underestimate the degree of synaptic loss by a few percentage points, as shown in Figure 25A. Considering the total synaptic losses over a wide range of the cochlea should help account for more of the discrepancy between ABR wave-1 amplitude and our estimates of fiber loss. But orphaned ribbons only account for a few percent, and it may be that the high amplitude ABR is more sensitive to low-SR fiber loss than simple synaptic counts. Additionally, synapses may appear intact by our histology but in fact be physiologically disconnected or otherwise damaged in ways we could not detect with the methods employed in this study.

The ABR amplitude is a product of both the number of fibers responding as well as how vigorously they respond to sound. In the frequency range over 16 kHz, the high-SR fibers have an average threshold around 20 dB SPL (Figure 8), and dynamic ranges of approximately 20 dB (Figure 12), meaning that their responses have fully saturated by around 40 dB SPL. Low-SR fibers on the other hand have thresholds as high as 65 dB SPL, and dynamic ranges as great as 40 dB – indicating that some low-SR fibers do not reach their maximum firing rate until stimulus intensity exceeds more than 100 dB SPL. Based on this line of reasoning, as stimulus intensity is increased over ~40 dB SPL, additional high-SR contribution comes only from the spread of excitation which will recruit off-frequency high-SR fibers but less so from increased firing rate. But just as the high-SR fibers begin to fully saturate, low- and med-SR fiber begin to respond, and their response will continue to grow stronger through the intensity range tested with ABR. As such, loss of nearly half of these low- and med-SR fibers should have a disproportionately large effect on the ABR at high intensities, accounting for the discrepancy between estimates of synaptic loss and the decrease in ABR wave-1 amplitudes.

6.3 Low-SR Losses

Schmiedt et al. showed that in aged gerbils there were missing low- and med-SR fibers in the high CF regions, declining from 57% to 29% of the population. Following the 2 hr exposure used in the present study, we see the low-SR population drop from 47% to 29%. Interestingly, the low-SR losses are similarly confined to the high frequency region, for CF > 6 kHz in gerbil and CF > 4 kHz our study. This may be relevant as our ribbon data show a basal spread of damage which is not restricted to a simple half-octave shift that has been well described (Cody and Johnstone, 1981; Robles and Ruggero, 2001). While the aged gerbils were never intentionally exposed to intense noise, the parallel loss of low-SR fibers in our sound exposed guinea pigs points toward a general susceptibility of low-SR fibers, particularly in the basal turns of the cochlea.

In the past, many have examined the effects of acoustic trauma but none have reported missing low-SR fibers (Liberman and Beil, 1979; Salvi et al., 1979). However, these studies were from animals with permanent threshold shifts, that are commonly accompanied by stereocilia loss on the IHCs (Liberman and Beil, 1979). Stereocilia loss reduces the SR of all fibers because of a decreased resting current into the IHC (Liberman and Dodds, 1984). Without the confound of stereocilia damage and permanent threshold shifts, we are able to see reduced numbers of low-SR fibers following our moderate sound exposure. This reinforces the fundamental differences in the mechanisms that create threshold shift versus changes in the supra-threshold properties seen in the present study.

One concern is that there is no way to know, with certainty, if the low- or high-SR fibers we record after exposure were of the same SR-type before exposure. These experiments present no method for measuring the same fiber before and after exposure. If low-SR fibers were becoming high-SR fibers we would expect to find more high-SR fibers with high thresholds. We see in Figure 11 that this is not the case, and the dependence of thresholds on SR has not changed. Another possibility is that low-SR fibers are actually still present, but inactive at the sound pressure level of the single fiber search stimulus. Schmiedt et. al. suggest that in their aged gerbils, a reduced endocochlear potential may lower the driving force into the IHC and affect the low-SR fibers preferentially (Schmiedt et al., 1996). In our study, the preservation of DPOAE responses suggests that the endocochlear potential has not changed. Furthermore, if a remaining fiber cannot respond to an intense noise burst, then it would likely have very little functional significance. Lastly, the loss of fibers (~20%) closely matches the loss of ribbons (~20%) in the high frequency regions, a correlation which suggests that the missing low-SR fibers found in this study reflect the neural degeneration seen in Lin et al. (2011). While it cannot be ruled out that low-SR fibers became high-SR fibers, the simplest interpretation is that fiber SRs have not changed but low-SR fibers were destroyed by the noise exposure.

6.4 Glutamate Excitotoxicity

Glutamate is an excitatory neurotransmitter found throughout the nervous system. While it serves many physiological functions, it has long been known to be neurotoxic at high doses (see for e.g. Lucas and Newhouse, 1957; Kostandy, 2012). The primary neurotransmitter at the IHC synapse widely presumed to be glutamate. Overstimulation of the cochlea causes excess glutamate release, whose excitotoxic effects trigger postsynaptic changes and degeneration (Puel et al., 1998; Kujawa and Liberman, 2006, 2009; Chen et al., 2009). Excessive glutamate stimulation results in increased influx of Ca^+ and Na^+ through the glutamate activated ion channels (Kostandy, 2012). When ion influx becomes excessive, it leads to a cascade of intracellular pathology that can damage or destroy the neuron. Osmotic pressures will cause water influx to follow the increased ion concentrations, directly causing terminal swelling. Application of glutamate agonists mimics the terminal swelling of noise exposure, and antagonists protect against it (Puel et al., 1998; Chen et al., 2009). The low-SR fibers may have certain physical disadvantages that make them less able survive this excitotoxic terminal swelling; they have different physical morphologies than the high-SR fibers. The dendritic endings of low-SR fibers tend to be long and thin, as much as half the diameter of high-SR fibers (Liberman, 1982; Gleich and Wilson, 1993), with similarly smaller synaptic endings. The lower amount of cell membrane may reduce the ability of a low-SR terminal to survive the physical swelling.

The sustained increase in intracellular postsynaptic Ca^+ causes its own toxic effects. Glutamate mediated influx of Ca^+ causes depolarization of the postsynaptic membrane, leading to the opening of additional voltage gated Ca^+ channels, increasing Ca^+ concentrations and compounding its cytotoxic effects. Increased Ca^+ activates cellular enzymatic pathways that cleave anti-apoptotic proteins and hydrolyze peptide bonds in cytoskeletal proteins which lead to vacuolization and neuronal death (Wang and Qin, 2010). Nonetheless, the post synaptic cell has to constantly handle calcium influx, and as such, small amounts of calcium are well buffered. In fact, calcium buffering in the cytoplasm is thought to be critical for precision of neural firing by regulating the time course of Ca^+ near the synapse (Roberts, 1993).

Ca^+ is also buffered by postsynaptic mitochondria, and this may be one of the primary pathways to control excess Ca^+ buildup (Carafoli, 2012). However, excess buildup of Ca^+ in the mitochondria has also been implicated in the release of apoptotic components and likely contributes to the neuronal death seen after noise exposure (Schild et al., 2003). Low-SR neurons have fewer mitochondria than their high-SR counterparts, perhaps because of lower metabolic demands associated with a weak spontaneous activity (Merchan-Perez and Liberman, 1996). This reduced number of mitochondria likely reduces the capacity to buffer excess calcium, making the low-SR fibers more susceptible to excitotoxic damage. This may help explain the loss of low-SR fibers following acoustic overexposure.

Overexposure may also affect expression of surface AMPA receptors for glutamate which are dynamically regulated, to help control the strength of synaptic transmission (Sheng and Lee, 2001). Expression of AMPA glutamate receptors on auditory nerve terminals decreases following acoustic overstimulation or application of glutamate receptor agonists (Chen et al., 2007). This may in fact be a protective mechanism, as blocking the endocytosis of receptors leads to increased excitotoxic damage (Chen et al., 2009). The present data show reduced staining volume for GluR2 (see Figure 23), suggesting that the AMPA receptors have decreased in size. Thus, the phenomenon of AMPA receptor endocytosis that has been shown in mouse may also occur in the guinea pig. The reduction in volume appears to be even across the entire IHC, implying that this phenomenon is not restricted to any SR-type but a common protective mechanism for all fibers to reduce the sensitivity of the post-synaptic neuron to glutamate, mitigating the excitotoxic effects.

6.5 Forward Masking

Relkin showed differences in forward masking between low and high SR fibers in chinchillas (Relkin and Doucet, 1991). We also show differences between low and high SR fibers in the guinea pig. Our data splits at approximately 100 ms recovery time: fibers with less than 100 ms recovery time are all high-SR, and fibers with greater than 100 ms recovery time are almost all low-SR. The difference between the fastest recovering fiber (~20 ms) and the slowest (4000 ms) is more than two orders of magnitude. This large difference and the clear separation between SR types would suggest that contributions from different SR types should be separable with gross physiology such as ABR or CAP.

Based on the analysis presented in Figure 18, losing low-SR fibers should increase masking at very short intervals. At long intervals, the only fibers contributing should be the low-SR fibers (as seen in the single fiber data of Figure 15). If there were no low-SR fibers at all, one might expect the CAP function to recover entirely by 100 ms, at which point high-SR fibers have fully recovered in Figure 13. It would appear that mean measures of forward masking are not sensitive enough to detect the partial loss of low-SR fibers in the present study. Schmiedt et al. (1996) did see their low-SR losses in CAP forward masking, however, they had greater losses of low-SR fibers in their gerbils.

The simplest explanation for the minimal effect from noise exposure on the CAP forward masked recovery functions is that while some low-SR fibers are missing, enough remain that we are unable to detect the differences with this test. Analysis of forward masking looks at the time course of recovery, and not the raw amplitude of the response. Normalized decrement functions serve to normalize the CAP responses to that animal's unmasked control condition. As such, the remaining ~60% of low- and med-SR fibers seem sufficient to provide unchanged, normalized CAP responses to forward masked stimuli when considered as group means. It is very likely that

one would see differences in the direction of low-SR fiber loss if CAP forward masking were measured in the same animal before and after exposure.

6.6 A Disrupted Synapse – Comparisons between Physiology and Morphology

At the healthy IHC synapse, there are clear levels of organization. Synaptic ribbons create an orderly arrangement at the basal surface of the IHC, particularly when viewed in cross section as seen in Figure 19 and Figure 21. Healthy IHCs have a decreasing gradient of ribbon size from modiolar to pillar sides of the IHC as assessed with CtBP2 staining (Figure 22). This gradient from large to small has been reported in immunohistochemistry in the mouse (Lieberman et al., 2011), and in ultrastructural EM studies in cat (Merchan-Perez and Liberman, 1996). There is also a decreasing gradient of receptor patch volume at the lower frequencies, though it does not appear to exist at 32 kHz (Figure 23G,H,I). Oddly, this gradient in receptor patch volume trends in the opposite direction from that seen in mouse where receptor patches get larger towards the pillar side of the IHC (Lieberman et al., 2011). This also differs from ultrastructural EM studies in cat that show larger post-synaptic densities on the modiolar side. However, differences in post-synaptic density size (Merchan-Perez and Liberman, 1996) are much smaller than the range of GluR2 staining volume (Lieberman et al., 2011). Liberman et al. speculate that this difference between GluR2 patch size and EM post-synaptic density size may be explained by expression of other glutamate receptors and receptor subunits (Lieberman et al., 2011). Unknown species differences in the expression of different glutamate receptors may explain why GluR2 receptor patch volume in the present study is smaller on the modiolar side of the IHC when other work suggests that they should be larger. It may or may not reflect the actual terminal size.

In addition to reduced synaptic ribbon counts (Figure 20), the size of synaptic ribbons was increased. The greatest change in ribbon volume (Figure 22 H, I) was on the pillar side of the IHC. This suggests that either small pillar-side ribbons have hypertrophied or large modiolar-side ribbons have migrated. In fact, increased ribbon volume has been previously reported in aged C57/Bl6 mice with congenital age-related hearing loss (Stamatakis et al., 2006). This may indicate that ribbon enlargement may be a common response to cochlear insult, but it is unknown if this enlargement is a pathologic condition or a compensatory mechanism to protect ribbons from the rigors of overstimulation. The increase in ribbon volume of our post-exposure ears did not increase the proportion of low-SR fibers, as one might have expected if ribbon size alone dictated spontaneous rate and if the correlation of ribbon size to SR-type seen in normal ears (Lieberman, 1982) was preserved. It is possible, however, that in addition to ribbon hypertrophy, that the low- and med-SR terminals have migrated and that the correlation between ribbon size and SR is lost in the sound exposed ear. Unpublished data from ouabain treated ears in mice shows that terminals and ribbons can migrate even in the adult ear

(Liberman, personal communication) supporting the idea that in addition to ribbon hypertrophy, there may be migration and reorganization of pre- and post-synaptic specializations in our noise traumatized ears. The selective loss of low- and med-SR fibers is not clearly represented in the morphology IHC innervation. The general dysmorphology of the exposed ear suggests that the excitotoxic effects of overstimulation may affect all synapses but is only lethal to the low- and med-SR fiber population.

7 Conclusions and Summary

In the two weeks following exposure to a moderate intensity noise exposure (106dB SPL, 4-8 kHz, 2hrs), guinea pigs suffer synaptic losses despite no change in cochlear threshold sensitivity. ABR amplitudes in response to high intensity tones are reduced, presynaptic ribbons and postsynaptic glutamate receptors are lost. The high-SR fibers are spared, and as they have the lowest thresholds this might help explain the preservation of threshold in light of the neuronal damage. Post exposure morphologic analysis revealed that disruption of the IHC synapse is complicated and may reflect synaptic changes to fibers of all SR-type. Single fiber recordings presented here suggest that the low- and med-SR fiber types are more susceptible to acoustic overexposure.

It is important to note that the degree of neuropathy seen in the present study was less than that seen in the mouse (Kujawa and Liberman, 2006), and less than seen previously in the guinea pig (Lin et al., 2011). The failure of the CAP forward masking data to show changes due to low-SR fiber loss may be due to incomplete losses of low-SR fibers. Future experiments utilizing multiple presentations of a sound exposure may more successfully ablate the entire low-SR population.

Possible evolutionary advantages can also be considered whereby preservation of threshold sensitivity from the high-SR fibers might provide advantages in hunting or avoiding predators. However, the irreversible loss of neurons and synaptic structures from this noise exposure are sobering. The data suggests that low-SR fiber loss and IHC synaptic pathology results from most acoustic overexposures in mammals and occurs at commonly encountered sound levels.

8 Acknowledgements

This work was supported in part by the NIH training grant awarded to the SHBT Program of the MIT-Harvard Division of Health Sciences and Technology (NIH T32 DC00038, and in part by research grants from the NIDCD: NIH R01 DC 000188 to Dr. M. Charles Liberman and NIH DC 008577 to Dr. Sharon Kujawa.

I would like to thank my thesis advisor, Dr. M. Charles Liberman, for his support and feedback in conducting experiments and generating strong scientific arguments. Thank you to the rest of the Liberman Lab, especially Ms. Ann Hickox for her immeasurable help discussing data, programming Matlab analysis, and dealing with the everyday difficulties of graduate school, and Leslie Liberman for her amazing micro-dissections. Special thanks to the rest of the Eaton-Peabody Laboratory and my SHBT classmates and teachers for their help and support over the past years.

I would like to thank my thesis committee, Dr. M. Christian Brown, Dr. Bertrand Delgutte, and Dr. Lisa Goodrich for their advice and comments on this dissertation.

I want to thank my parents for always encouraging me to pursue my scientific endeavors, no matter how complicated or challenging.

Last, but not least, I want to thank my wife Ronit, for all of her support, encouragement and love while I worked on my PhD.

9 List of References

Buran BN, Strenzke N, Neef A, Gundelfinger ED, Moser T, Liberman MC. Onset coding is degraded in auditory nerve fibers from mutant mice lacking synaptic ribbons. *The Journal of Neuroscience* 30: 7587–97, 2010.

Carafoli E. The interplay of mitochondria with calcium: An historical appraisal. *Cell Calcium* 52: 1–8, 2012.

Chen Z, Kujawa SG, Sewell WF. Auditory sensitivity regulation via rapid changes in expression of surface AMPA receptors. *Nature Neuroscience* 10: 1238–40, 2007.

Chen Z, Peppi M, Kujawa SG, Sewell WF. Regulated expression of surface AMPA receptors reduces excitotoxicity in auditory neurons. *Journal of Neurophysiology* 102: 1152–9, 2009.

Chung D, Mack B. The effect of masking by noise on word discrimination scores in listeners with normal hearing and with noise-induced hearing loss. *Scandinavian Audiology* 8: 139–143, 1979.

Cody AR, Johnstone BM. Acoustic trauma: single neuron basis for the “half-octave shift”. *The Journal of the Acoustical Society of America* 70: 707–11, 1981.

Furman AC, Avissar M, Saunders JC. The effects of intense sound exposure on phase locking in the chick (*Gallus domesticus*) cochlear nerve. *The European Journal of Neuroscience* 24: 2003–10, 2006.

Gates GA, Schmid P, Kujawa SG, Nam B, D’Agostino R. Longitudinal threshold changes in older men with audiometric notches. *Hearing research* 141: 220–8, 2000.

Geisler CD. *From Sound to Synapse: Physiology of the Mammalian Ear.* Oxford University Press, USA, 1998.

Gleich O, Wilson S. The diameters of guinea pig auditory nerve fibres: distribution and correlation with spontaneous rate. *Hearing Research* 71: 69–79, 1993.

Glowatzki E, Grant L, Fuchs P. Hair cell afferent synapses. *Current Opinion in Neurobiology* 18: 389–95, 2008.

Harris DMM, Dallos P. Forward masking of auditory nerve fiber responses. *Journal of Neurophysiology* 42: 1083–1107, 1979.

Hashimoto S, Kimura RS, Takasaka T. Computer-aided three-dimensional reconstruction of the inner hair cells and their nerve endings in the guinea pig cochlea. *Acta Oto-laryngologica* 109: 228–34, 1990.

Husbands JM, Steinberg S a, Kurian R, Saunders JC. Tip-link integrity on chick tall hair cell stereocilia following intense sound exposure. *Hearing Research* 135: 135–45, 1999.

Khimich D, Nouvian R, Pujol R, tom Dieck S, Egner A, Gundelfinger ED, Moser T. Hair cell synaptic ribbons are essential for synchronous auditory signalling. *Nature* 434: 889–894, 2005.

Kiang NY, Moxon EC, Levine RA. Auditory-nerve activity in cats with normal and abnormal cochleas. In: Sensorineural hearing loss. *Ciba Foundation symposium*. .

Kiang NY. *Discharge patterns of single fibers in the cat's auditory nerve*. M.I.T. Press, 1965.

Kostandy BB. The role of glutamate in neuronal ischemic injury: the role of spark in fire. *Neurological Sciences : Official Journal of the Italian Neurological Society and of the Italian Society of Clinical Neurophysiology* 33: 223–37, 2012.

Kujawa SG, Liberman MC. Acceleration of age-related hearing loss by early noise exposure: evidence of a misspent youth. *The Journal of Neuroscience* 26: 2115–23, 2006.

Kujawa SG, Liberman MC. Adding insult to injury: cochlear nerve degeneration after “temporary” noise-induced hearing loss. *The Journal of Neuroscience* 29: 14077–85, 2009.

Liberman LD, Wang H, Liberman MC. Opposing gradients of ribbon size and AMPA receptor expression underlie sensitivity differences among cochlear-nerve/hair-cell synapses. *The Journal of neuroscience* 31: 801–8, 2011.

Liberman M, Chesney CP, Kujawa SG. Effects of Selective Inner Hair Cell Loss on DPOAE and CAP in Carboplatin-Treated Chinchillas. *Auditory Neuroscience* 3: 255–268, 1997.

Liberman MC, Beil DG. Hair cell condition and auditory nerve response in normal and noise-damaged cochleas. *Acta Oto-laryngologica* 88: 161–76, 1979.

Liberman MC, Dodds LW. Single-neuron labeling and chronic cochlear pathology. III. Stereocilia damage and alterations of threshold tuning curves. *Hearing Research* 16: 55–74, 1984.

Liberman MC. Auditory-nerve response from cats raised in a low-noise chamber. *The Journal of the Acoustical Society of America* 63: 442–55, 1978.

Liberman MC. Morphological differences among radial afferent fibers in the cat cochlea: an electron-microscopic study of serial sections. *Hearing Research* 3: 45–63, 1980.

Liberman MC. Single-neuron labeling in the cat auditory nerve. *Science* 216: 1239, 1982.

Lin HW, Furman AC, Kujawa SG, Liberman MC. Primary Neural Degeneration in the Guinea Pig Cochlea After Reversible Noise-Induced Threshold Shift. *Journal of the Association for Research in Otolaryngology* 616: 605–616, 2011.

Lonsbury-Martin BL, Martin GK. The clinical utility of distortion-product otoacoustic emissions. *Ear and Hearing* 11: 144–54, 1990.

Lucas DR, Newhouse JP. The toxic effect of sodium L-glutamate on the inner layers of the retina. *A.M.A. Archives of Ophthalmology* 58: 193–201, 1957.

Merchan-Perez a, Liberman MC. Ultrastructural differences among afferent synapses on cochlear hair cells: correlations with spontaneous discharge rate. *The Journal of Comparative Neurology* 371: 208–21, 1996.

Nouvian R, Beutner D, Parsons TD, Moser T. Structure and function of the hair cell ribbon synapse. *The Journal of Membrane Biology* 209: 153–65, 2006.

OSHA. Occupational noise exposure. - 1910.95 [Online]. 2012. <http://www.osha.gov> [25 Aug. 2012].

Prijs VF. Single-unit response at the round window of the guinea pig. *Hearing Research* 21: 127–33, 1986.

Puel JL, Ruel J, Gervais d'Aldin C, Pujol R. Excitotoxicity and repair of cochlear synapses after noise-trauma induced hearing loss. *Neuroreport* 9: 2109–14, 1998.

Pujol R, Puel JLUC. Excitotoxicity, synaptic repair, and functional recovery in the mammalian cochlea: a review of recent findings. *Annals of the New York Academy of Sciences* 884: 249–254, 1999.

Relkin EM, Doucet JR, Sterns A. Evidence for a slow component that reflects recovery of low spontaneous-rate auditory neurons. *Hearing Research* 83: 183–189, 1995.

Relkin EM, Doucet JR. Recovery from prior stimulation. I: Relationship to spontaneous firing rates of primary auditory neurons. *Hearing Research* 55: 215–22, 1991.

Relkin EM, Smith RL. Forward masking of the compound action potential: thresholds for the detection of the N1 peak. *Hearing Research* 53: 131–40, 1991.

Relkin EM, Turner CW. A reexamination of forward masking in the auditory nerve. *The Journal of the Acoustical Society of America* 84: 584–91, 1988.

Roberts WM. Spatial calcium buffering in saccular hair cells. *Nature* 363: 74–6, 1993.

Robertson D. Effects of acoustic trauma on stereocilia structure and spiral ganglion cell tuning properties in the guinea pig cochlea. *Hearing Research* 7: 55–74, 1982.

- Robles L, Ruggero MA.** Mechanics of the mammalian cochlea. *Physiological Reviews* 81: 1305–52, 2001.
- Salvi RJ, Hamernik RP, Henderson D.** Auditory nerve activity and cochlear morphology after noise exposure. *Archives of oto-rhino-laryngology* 224: 111–6, 1979.
- Saunders GH, Haggard MP.** The clinical assessment of obscure auditory dysfunction-1. Auditory and psychological factors. *Ear and hearing* 10: 200, 1989.
- Schild L, Huppelsberg J, Kahlert S, Keilhoff G, Reiser G.** Brain mitochondria are primed by moderate Ca²⁺ rise upon hypoxia/reoxygenation for functional breakdown and morphological disintegration. *The Journal of Biological Chemistry* 278: 25454–60, 2003.
- Schmiedt RA, Mills JH, Boettcher FA.** Age-related loss of activity of auditory-nerve fibers. *Journal of Neurophysiology* 76: 2799–803, 1996.
- Schuknecht H.** Hearing Losses Following Partial Section of the Cochlear Nerve. *The Laryngoscope* 63: 441, 1953.
- Sheng M, Lee SH.** AMPA receptor trafficking and the control of synaptic transmission. *Cell* 105: 825–8, 2001.
- Spassova M a., Avissar M, Furman AC, Crumling M a., Saunders JC, Parsons TD.** Evidence That Rapid Vesicle Replenishment of the Synaptic Ribbon Mediates Recovery from Short-Term Adaptation at the Hair Cell Afferent Synapse. *Journal of the Association for Research in Otolaryngology* 5: 376–390, 2004.
- Stamatakis S, Francis HW, Lehar M, May BJ, Ryugo DK.** Synaptic alterations at inner hair cells precede spiral ganglion cell loss in aging C57BL/6J mice. *Hearing Research* 221: 104–18, 2006.
- Taberner AM, Liberman MC.** Response properties of single auditory nerve fibers in the mouse. *Journal of Neurophysiology* 93: 557–69, 2005.
- Tsuji J, Liberman MC.** Intracellular labeling of auditory nerve fibers in guinea pig: central and peripheral projections. *The Journal of Comparative Neurology* 381: 188–202, 1997.
- Wang Y, Qin Z-H.** Molecular and cellular mechanisms of excitotoxic neuronal death. *Apoptosis* 15: 1382–402, 2010.
- Westerman L a, Smith RL.** Rapid and short-term adaptation in auditory nerve responses. *Hearing Research* 15: 249–60, 1984.